PTEP

Prog. Theor. Exp. Phys. **2021**, 103B07 (24 pages)
DOI: 10.1093/ptep/ptab121

General one-loop contributions to the decay $H \to \nu_l \bar{\nu}_l \gamma$

Khiem Hong Phan[1,2,*], Le Tho Hue, and Dzung Tri Tran[4]

[1]*Institute of Fundamental and Applied Sciences, Duy Tan University, Ho Chi Minh City* 700000*, Vietnam*
[2]*Faculty of Natural Sciences, Duy Tan University, Da Nang City* 550000*, Vietnam*
[3]*Institute of Physics, Vietnam Academy of Science and Technology,* 10 *Dao Tan, Ba Dinh, Hanoi, Vietnam*
[4]*University of Science Ho Chi Minh City,* 227 *Nguyen Van Cu, District* 5*, Ho Chi Minh City, Vietnam*
[*]E-mail: phanhongkhiem@duytan.edu.vn

Received June 29, 2021; Revised September 5, 2021; Accepted September 20, 2021; Published October 5, 2021

General one-loop contributions to the decay amplitudes $H \to \nu_l \bar{\nu}_l \gamma$ are presented, considering all possible contributions of additional heavy vector gauge bosons, fermions, and charged (and also neutral) scalar particles appearing in the loop diagrams. Moreover, the results can be applied directly when extra neutrinos (apart from three ones in the standard model) are taken into account in final states. Analytic results are expressed in terms of Passarino–Veltman scalar functions which can be evaluated numerically using `LoopTools`. In the standard model framework, these analytical results are generated and cross-checked with previous computations. We find that our results are well consistent with these computations. Within the standard model limit, phenomenological results for the decay channels are also studied using the present input parameters at the Large Hadron Collider. Lastly, the calculation is also applied to the Two Higgs Doublet Model framework as another example.

Subject Index B53, B59

1. Introduction

Searching for all decay modes of the standard model-like (SM-like) Higgs boson is one of the main purposes of the High Luminosity Large Hadron Collider (HL-LHC) [1,2] as well as Future Lepton Colliders [3], because the partial decay widths of the Higgs boson contain an important information for testing the nature of Higgs sector. Among the Higgs decay modes, the channels of $H \to$ invisible particles [4–10] and $H \to \gamma$ plus invisible particles [11,12] are greatly of interest, for the following reasons. First, these decay processes can be measured at the LHC [4–6,8,11,12]. Therefore, they could be used for verifying the SM at higher energy regions. On the other hand, there exist many theories beyond the standard models (BSM) in which new invisible particles rather than neutrinos are proposed. In addition, many new heavy particles that are absent from the SM may exchange in the loop diagrams of the aforementioned decay channels. As a result, the decay widths of $H \to \nu_l \bar{\nu}_l \gamma$ could provide an useful tool for controlling the SM background as well as constraining new physical parameters.

One-loop formulas for $H \to \nu_l \bar{\nu}_l \gamma$ within the SM framework have been computed in Ref. [13]. Besides that, an independent model for investigating Higgs decay to a photon and invisible particles has been proposed in Ref. [14]. The decay channel of Higgs to a photon and the light vector gauge bosons which they belong to $U(1)$ extension of the SM has also considered in Ref. [15]. In a next-to-minimal supersymmetry (SUSY) framework, Higgs decay to a photon plus a pair of lightest SUSY particles was studied in Ref. [16]. In Ref. [16], the decay process was used to probe dark matter

Funded by SCOAP[3]

as well as constraining SUSY parameters. The supersymmetry-breaking scale has been examined through the Higgs decay to a photon and gravitinos in [17].

In this article, we present general one-loop formulas for the decay $H \to \nu_l \bar{\nu}_l \gamma$. The results are valid for many BSMs; new heavy vector bosons, fermions, and scalar particles predicted by these models are considered in the loop diagrams. Moreover, the calculations can be extended directly when the extra neutrinos (rather than 3 in SM) are taken into account in final states. Analytic results are expressed in terms of Passarino–Veltman (PV) scalar functions which can be computed numerically using the package `LoopTools`. The calculations are also verified numerically by checking the ultraviolet (UV) finiteness of the results. We find that the results are in good stability when varying UV cutoff parameters. The results are then applied to the case of the SM and the decay widths are generated and cross-checked with the previous computations. Our results in this work are in good agreement with the previous references. All physical results for the decay channels within the SM are examined using the present input parameters at the LHC. Lastly, the calculation is also applied to the Two Higgs Doublet Model (THDM) framework [18]. The phenomenological analysis for the decay processes in several BSMs are referred to our next papers.

The results of this work can be applied to calculate one-loop contributions of new particles predicted by well-known BSMs constructed previously, for example, many popular SM extensions that include only new charged scalars such as THDM [18]. In the SUSY model, new loop contributions come from charged Higgs bosons, superpartners of leptons and gauge bosons. One-loop contributions from new charged gauge bosons may appear in many electroweak gauge extensions such as the left–right models (LR) constructed from $SU(2)_L \times SU(2)_R \times U(1)_Y$ [19–21], the 3-3-1 models ($SU(3)_L \times U(1)_X$) [22–28], the 3-4-1 models ($SU(4)_L \times U(1)_X$) [28–33], etc. These one-loop contributions may be significant in the amplitudes of the mentioned decay processes. Phenomenological results for the decay processes in the above models will be very interesting for further studies, which will be our future projects.

The layout of the paper is as follows: In Sect. 2, we briefly present the one-loop tensor reduction method. Detailed calculations for one-loop contributions to $H \to \nu_l \bar{\nu}_l \gamma$ are also presented in this section, as are the applications of this work to the SM and THDM. Conclusions and outlook are detailed Sect. 3. In the appendices, Feynman rules and couplings involved in the decay processes are shown. Further, checks for the calculation are discussed and we also briefly review THDM in the appendices.

2. Calculation

Detailed calculations for one-loop contributions to $H \to \nu_l \bar{\nu}_l \gamma$ are presented in this section. We first briefly describe the one-loop tensor reduction method in the following subsection. General analytic results and physical results of the decay processes are then shown in the next subsections.

2.1. Method

In this calculation, we follow the tensor reduction method developed in Ref. [34]. Following this technique, tensor one-loop integrals with N-external lines can be decomposed into scalar functions with $N \leq 4$. The approach will be explained briefly in the following paragraphs.

First, one-loop one-, two-, three- and four-point tensor integrals with rank P are defined:

$$\{A; B; C; D\}^{\mu_1 \mu_2 \cdots \mu_P} = (\mu^2)^{2-d/2} \int \frac{d^d k}{(2\pi)^d} \frac{k^{\mu_1} k^{\mu_2} \cdots k^{\mu_P}}{\{D_1; D_1 D_2; D_1 D_2 D_3; D_1 D_2 D_3 D_4\}}. \quad (1)$$

In this formula, D_j ($j = 1, \cdots, 4$) are the inverse Feynman propagators which are given as

$$D_j = (k + q_j)^2 - m_j^2 + i\rho, \tag{2}$$

where $q_j = \sum_{i=1}^{j} p_i$, p_i are the external momenta and m_j are internal masses in the loops. Dimensional regularization is performed in the space–time dimension $d = 4 - 2\varepsilon$. The parameter μ^2 plays the role of a renormalization scale. If the numerators of the integrands in Eq. (1) become 1, we have scalar one-loop one-, two-, three- and four-point integrals [34] (they are called the A_0, B_0, C_0 and D_0 functions). We then present the explicit reduction formulas for one-loop one-, two-, three- and four-point tensor integrals up to rank $P = 3$ as follows [34]:

$$A^\mu = 0, \tag{3}$$

$$A^{\mu\nu} = g^{\mu\nu} A_{00}, \tag{4}$$

$$A^{\mu\nu\rho} = 0, \tag{5}$$

$$B^\mu = q^\mu B_1, \tag{6}$$

$$B^{\mu\nu} = g^{\mu\nu} B_{00} + q^\mu q^\nu B_{11}, \tag{7}$$

$$B^{\mu\nu\rho} = \{g, q\}^{\mu\nu\rho} B_{001} + q^\mu q^\nu q^\rho B_{111}, \tag{8}$$

$$C^\mu = q_1^\mu C_1 + q_2^\mu C_2 = \sum_{i=1}^{2} q_i^\mu C_i, \tag{9}$$

$$C^{\mu\nu} = g^{\mu\nu} C_{00} + \sum_{i,j=1}^{2} q_i^\mu q_j^\nu C_{ij}, \tag{10}$$

$$C^{\mu\nu\rho} = \sum_{i=1}^{2} \{g, q_i\}^{\mu\nu\rho} C_{00i} + \sum_{i,j,k=1}^{2} q_i^\mu q_j^\nu q_k^\rho C_{ijk}, \tag{11}$$

$$D^\mu = q_1^\mu D_1 + q_2^\mu D_2 + q_3^\mu D_3 = \sum_{i=1}^{3} q_i^\mu D_i, \tag{12}$$

$$D^{\mu\nu} = g^{\mu\nu} D_{00} + \sum_{i,j=1}^{3} q_i^\mu q_j^\nu D_{ij}, \tag{13}$$

$$D^{\mu\nu\rho} = \sum_{i=1}^{3} \{g, q_i\}^{\mu\nu\rho} D_{00i} + \sum_{i,j,k=1}^{3} q_i^\mu q_j^\nu q_k^\rho D_{ijk}. \tag{14}$$

The short notation [34] $\{g, q_i\}^{\mu\nu\rho}$ is used as follows in the above relations: $\{g, q_i\}^{\mu\nu\rho} = g^{\mu\nu} q_i^\rho + g^{\nu\rho} q_i^\mu + g^{\mu\rho} q_i^\nu$. The scalar coefficients $A_{00}, B_1, \cdots, D_{333}$ in the right-hand sides of the above equations are so-called PV functions [34]. Analytic formulas of the PV functions are well-known and they have been implemented into `LoopTools` [35] for numerical computations.

2.2. *General one-loop contributions to $H \to \nu_l \bar{\nu}_l \gamma$*

General one-loop contributions to $H(p) \to \nu_l(q_1)\bar{\nu}_l(q_2)\gamma(q_3)$ arbitrarily beyond the SMs are calculated in this subsection. One-loop Feynman diagrams involving the decay processes in the unitary

gauge can be grouped into several classes shown in the following paragraphs. For an on-shell external photon, the ward identity is implied. As a result, we apply the relation $q_3^\nu \epsilon_\nu^* = 0$ for simplifying the amplitudes, where q_3^ν, ϵ_ν^* are the momentum and the polarization vector of the external photon, respectively. Kinematic invariant variables involved in the decay processes are included:

$$\begin{aligned} &p^2 = M_H^2, \quad q_1^2 = q_2^2 = q_3^2 = 0, \\ &q_{12} = q^2 = (q_1 + q_2)^2 = 2q_1 \cdot q_2, \quad q_{13} = 2q_1 \cdot q_3, \quad q_{23} = 2q_2 \cdot q_3. \end{aligned} \tag{15}$$

The general one-loop amplitude which obeys the structure of the Lorentz invariance can be decomposed as follows [36]:

$$\mathcal{A}_{\text{loop}} = \sum_{k=1}^{2} \left\{ [q_3^\mu q_k^\nu - g^{\mu\nu} q_3 \cdot q_k] \bar{u}(q_1)(F_{k,R}\gamma_\mu P_R + F_{k,L}\gamma_\mu P_L) v(q_2) \right\} \varepsilon_\nu^*. \tag{16}$$

In this equation, all form factors are computed as follows:

$$F_{k,L/R} = F_{k,L/R}^{\text{Trig}} + F_{k,L/R}^{\text{Box}} \tag{17}$$

for $k = 1, 2$. Each form factor in (16) will be contributed to by different kind of particles such as vector bosons V_i, charged scalar particles S_i and fermions f_i exchanging in loop diagrams. These particles appear in many BSMs, the Feynman rules of which are collected in Table C.1; all their couplings are generalized as in Table C.2. After using them to write down all one-loop contributions to the decay amplitudes, the `Package-X` [37] will be used to contract all Dirac traces in the general dimension d. The analytic formulas of all one-loop contributions will then be decomposed into one-loop tensor integrals. In this step, the above tensor reduction method is employed to transform all tensor integrals into scalar functions included in the form factors $F_{k,L/R}$. Finally, they are collected as functions of the well-known PV scalar coefficients [34,35].

2.2.1. *One-loop triangle diagrams*

We are going to present the calculation in detail. We first arrive at the contributions of one-loop triangle diagrams by exchanging vector bosons V_i, V_j in the loop (seen Fig. 1).

By applying one-loop tensor reduction method in the previous subsection, the form factors are expressed in terms of PV-functions as follows:

$$\begin{aligned} F_{k,L}^{\text{Trig}}|_{V_i,V_j} = &\sum_{V_i,V_j} \frac{g_{HViVj}\, g^L_{V_k^0 \nu_l \bar{\nu}_l}}{32\pi^2 M_{V_i}^2 M_{V_j}^2 (q^2 - M_{V_k^0}^2 + i\Gamma_{V_k^0} M_{V_k^0})} \\ &\times \Big\{ \Big[eQg_{V_k^0 V_i V_j}(M_H^2 + M_{V_i}^2 + M_{V_j}^2) + 2g_{V_k^0 A V_i V_j}(M_H^2 - M_{V_i}^2) \Big] B_{11}(M_H^2, M_{V_j}^2, M_{V_i}^2) \\ &+ \Big[eQg_{V_k^0 V_i V_j}(M_H^2 - M_{V_i}^2 + 3M_{V_j}^2) - 2g_{V_k^0 A V_i V_j} M_{V_j}^2 \Big] B_1(M_H^2, M_{V_j}^2, M_{V_i}^2) \\ &+ 2M_{V_j}^2 \Big[eQg_{V_k^0 V_i V_j} - g_{V_k^0 A V_i V_j} \Big] B_0(M_H^2, M_{V_j}^2, M_{V_i}^2) \\ &+ 2g_{V_k^0 A V_i V_j} \Big[M_H^2 B_{111} + B_{00} + 2B_{001} \Big](M_H^2, M_{V_j}^2, M_{V_i}^2) \\ &+ 4eQg_{V_k^0 V_i V_j} M_{V_j}^2 \Big(3M_{V_i}^2 + M_{V_j}^2 - q^2 \Big) C_0(0, q^2, M_H^2, M_{V_j}^2, M_{V_j}^2, M_{V_i}^2) \end{aligned}$$

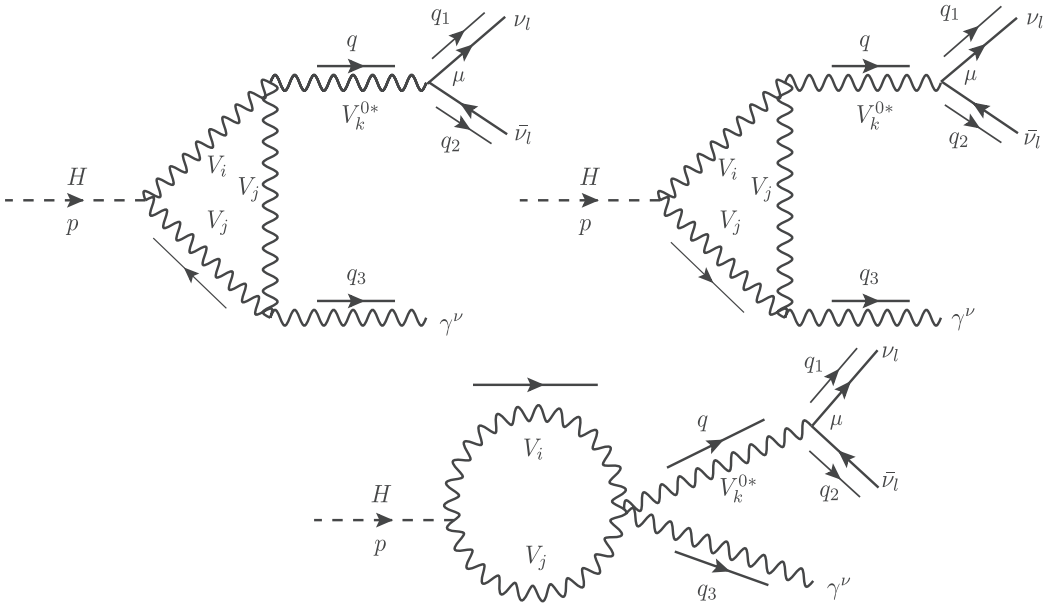

Fig. 1. One-loop triangle diagrams with exchanging vector bosons $V_{i,j}$ particles in the loop.

$$
\begin{aligned}
&+ 2eQg_{V_k^0 V_i V_j}\Big[M_H^2(M_{V_i}^2 + M_{V_j}^2 - q^2) + (4d-6)M_{V_i}^2 M_{V_j}^2 + M_{V_i}^4 + M_{V_j}^4 \\
&- q^2(M_{V_i}^2 + M_{V_j}^2)\Big](C_{22} + C_{12})(0, q^2, M_H^2, M_{V_j}^2, M_{V_j}^2, M_{V_i}^2) \\
&+ 2eQg_{V_k^0 V_i V_j}\Big[M_H^2(M_{V_i}^2 + M_{V_j}^2 - q^2) + (4d-6)M_{V_i}^2 M_{V_j}^2 + 3M_{V_j}^4 \\
&- M_{V_i}^4 + q^2(M_{V_i}^2 - 3M_{V_j}^2)\Big]C_2(0, q^2, M_H^2, M_{V_j}^2, M_{V_j}^2, M_{V_i}^2)\Big\}, \qquad (18)
\end{aligned}
$$

$$
F_{k,R}^{\text{Trig}}|_{V_i,V_j} = F_{k,L}^{\text{Trig}}|_{V_i,V_j}(g^L_{V_k^0 \nu_l \bar{\nu}_l} \to g^R_{V_k^0 \nu_l \bar{\nu}_l}). \qquad (19)
$$

We note that the form factors follow the relation $F_{k,L/R}^{\text{Trig}} = F_{1,L/R}^{\text{Trig}} = F_{2,L/R}^{\text{Trig}}$, and $F_{k,R}^{\text{Trig}}|_{V_i,V_j}$ can be obtained directly by replacing $g^L_{V_k^0 \nu_l \bar{\nu}_l} \to g^R_{V_k^0 \nu_l \bar{\nu}_l}$ in $F_{k,L}^{\text{Trig}}|_{V_i,V_j}$ (as shown in Eq. 18).

We next take into account the attributions of one-loop triangle graphs in which a boson V_i and two charged scalar particles S_j are internal lines (as shown in Fig. 2). Applying the same procedure, the form factors read:

$$
\begin{aligned}
F_{k,L}^{\text{Trig}}|_{V_i,S_j} = &\sum_{Vi,Sj} \frac{eQg_{HV_iS_j}\, g_{V_k^0 V_i S_j}\, g^L_{V_k^0 \nu_l \bar{\nu}_l}}{8\pi^2 M_{V_i}^2 (q^2 - M_{V_k^0}^2 + i\Gamma_{V_k^0} M_{V_k^0})} \\
&\times \Big\{(M_{S_j}^2 - M_{V_i}^2 - M_H^2)\Big[C_{22} + C_{12}\Big](0, q^2, M_H^2, M_{S_j}^2, M_{S_j}^2, M_{V_i}^2) \\
&+ (M_{S_j}^2 + M_{V_i}^2 - M_H^2)\; C_2(0, q^2, M_H^2, M_{S_j}^2, M_{S_j}^2, M_{V_i}^2)\Big\}, \qquad (20)
\end{aligned}
$$

$$
F_{k,R}^{\text{Trig}}|_{V_i,S_j} = F_{k,L}^{\text{Trig}}|_{V_i,S_j}(g^L_{V_k^0 \nu_l \bar{\nu}_l} \to g^R_{V_k^0 \nu_l \bar{\nu}_l}). \qquad (21)
$$

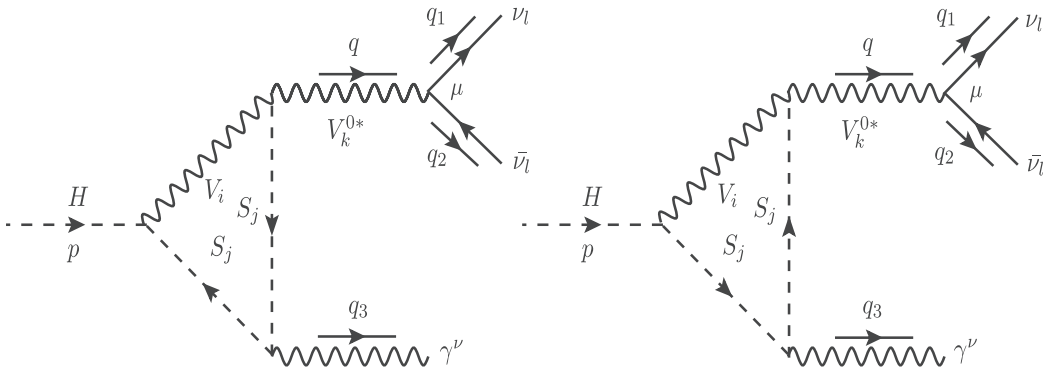

Fig. 2. One-loop triangle diagrams with a vector boson V_i and two scalar bosons S_j exchanging in the loop.

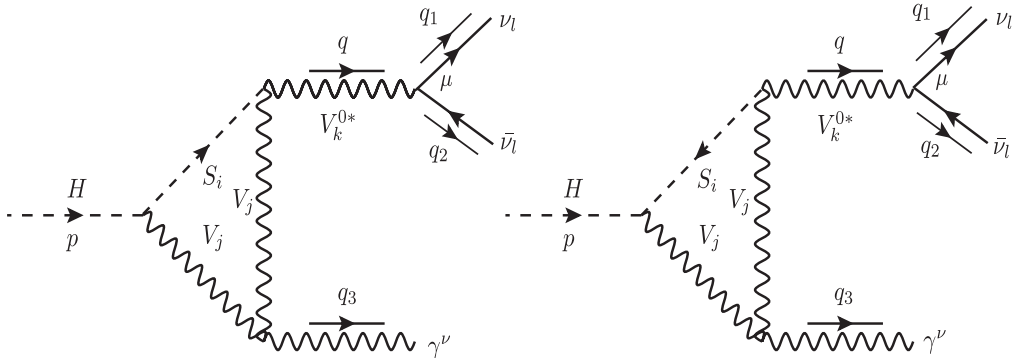

Fig. 3. One-loop triangle diagrams with two vector bosons V_j and a scalar boson S_i in the loop.

In addition, we have two vector bosons V_j and a charged scalar S_i exchanging in one-loop triangle diagrams (as described as in Fig. 3). In the same manner as the above procedure, the form factors $F^{\rm Trig}_{k,L/R}$ are presented as functions of PV coefficients:

$$F^{\rm Trig}_{k,L}|_{S_i,V_j} = \sum_{S_i,V_j} \frac{eQg_{HS_iV_j}\, g_{V_k^0 S_i V_j}\, g^L_{V_k^0 \nu_l \bar{\nu}_l}}{16\pi^2 M^2_{V_j}(q^2 - M^2_{V_k^0} + i\Gamma_{V_k^0} M_{V_k^0})} \times \Big\{ (M_H^2 - M^2_{S_i} + M^2_{V_j})\Big[C_{22} + C_{12} + C_2\Big](0, q^2, M_H^2, M^2_{V_j}, M^2_{V_j}, M^2_{S_i}) + 2M^2_{V_j}\Big[C_2 + C_0\Big](0, q^2, M_H^2, M^2_{V_j}, M^2_{V_j}, M^2_{S_i})\Big\}, \tag{22}$$

$$F^{\rm Trig}_{k,R}|_{S_i,V_j} = F^{\rm Trig}_{k,L}|_{S_i,V_j}(g^L_{V_k^0 \nu_l \bar{\nu}_l} \to g^R_{V_k^0 \nu_l \bar{\nu}_l}). \tag{23}$$

Further, we also mention the attributions of one-loop bubble and triangle diagrams with both charged scalar bosons S_i, S_j in the loop (as depicted in Fig. 4). The result for the form factors $F^{\rm Trig}_{k,L/R}$ reads

$$F^{\rm Trig}_{k,L}|_{S_i,S_j} = \sum_{S_i,S_j} \frac{eQg_{HS_iS_j}\, g_{V_k^0 S_i S_j}\, g^L_{V_k^0 \nu_l \bar{\nu}_l}}{4\pi^2(q^2 - M^2_{V_k^0} + i\Gamma_{V_k^0} M_{V_k^0})}\Big[C_{22} + C_{12} + C_2\Big](0, q^2, M_H^2, M^2_{S_j}, M^2_{S_j}, M^2_{S_i}), \tag{24}$$

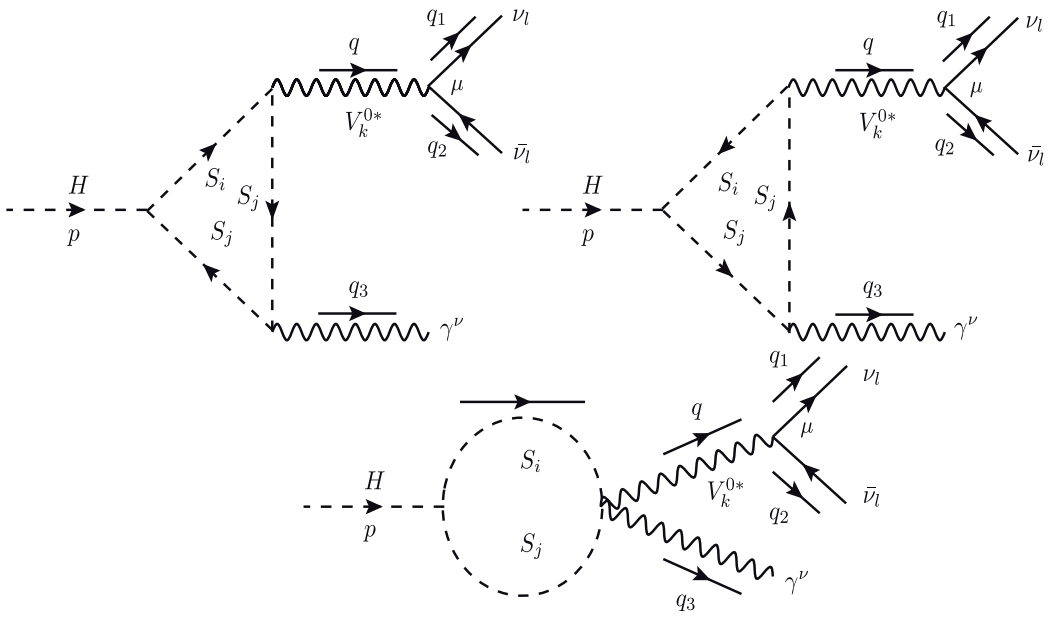

Fig. 4. One-loop bubble and triangle diagrams with all charged scalar bosons $S_{i,j}$ internal lines.

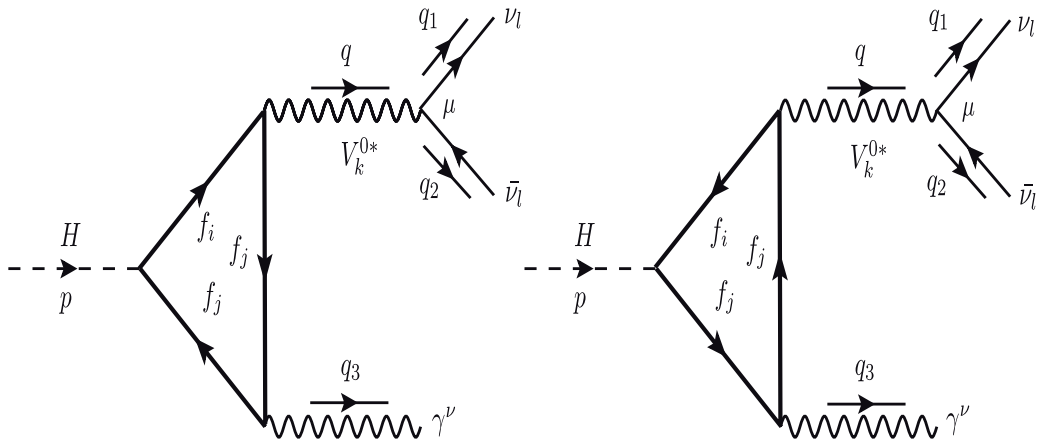

Fig. 5. Feynman triangle diagrams with fermion $f_{i/j}$ particles exchanging in the loop.

$$F^{\text{Trig}}_{k,R}|_{S_i,S_j} = F^{\text{Trig}}_{k,L}|_{S_i,S_j}(g^L_{V^0_k\nu_l\bar{\nu}_l} \to g^R_{V^0_k\nu_l\bar{\nu}_l}). \tag{25}$$

Lastly, we also have fermions exchanging in the loop of the triangle Feynman diagrams which are depicted in Fig. 5. The form factors $F^{\text{Trig}}_{k,L/R}$ for fermion $f_{i/j}$ contributions can be expressed as follows:

$$\begin{aligned} F^{\text{Trig}}_{k,L}|_{f_i,f_j} = \sum_{f_i,f_j} & \frac{eQ_f N^f_C\, g^L_{V^0_k\nu_l\bar{\nu}_l}}{16\pi^2(q^2 - M^2_{V^0_k} + i\Gamma_{V^0_k}M_{V^0_k})} \\ & \times \Big\{(g^L_{Hf_if_j} + g^R_{Hf_if_j})(g^L_{V^0_kf_if_j} + g^R_{V^0_kf_if_j}) \\ & \times \Big[2(m_{f_i} + m_{f_j})\Big(C_{22} + C_{12}\Big)(0, q^2, M^2_H, m^2_{f_j}, m^2_{f_j}, m^2_{f_i}) \end{aligned}$$

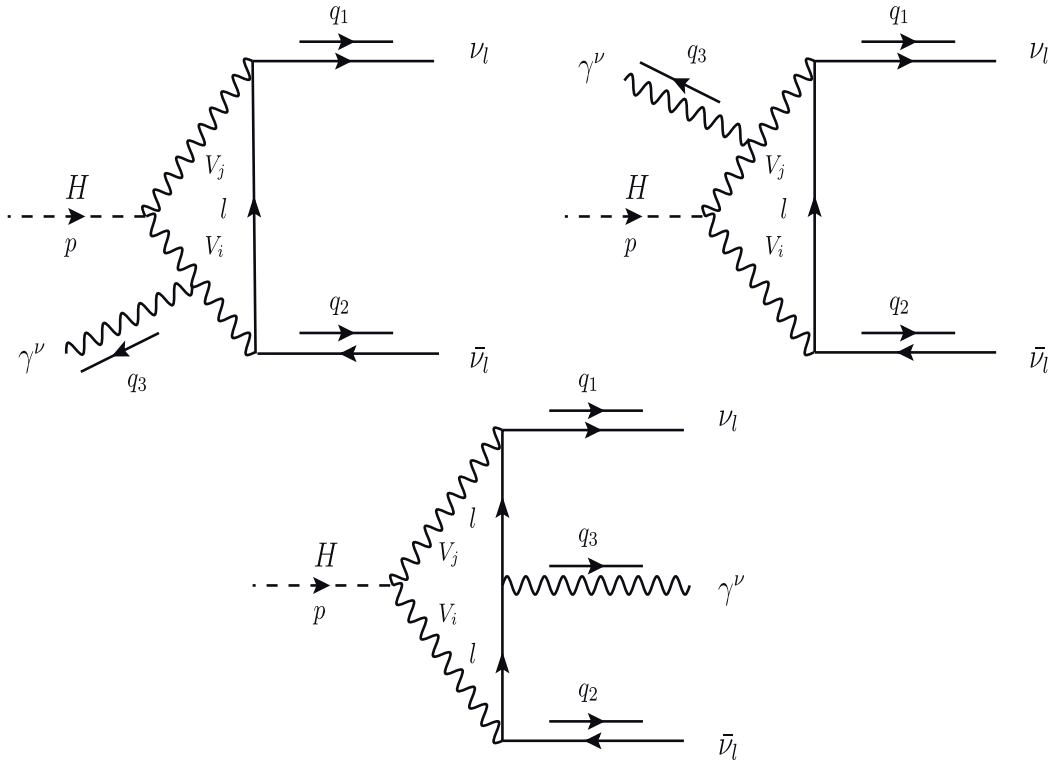

Fig. 6. One-loop box diagrams with V_i, V_j exchanging in the loop.

$$
\begin{aligned}
&+ (m_{f_i} + 3m_{f_j}) C_2(0, q^2, M_H^2, m_{f_j}^2, m_{f_j}^2, m_{f_i}^2) + m_{f_j} C_0(0, q^2, M_H^2, m_{f_j}^2, m_{f_j}^2, m_{f_i}^2) \Big] \\
&+ (g^R_{Hf_if_j} - g^L_{Hf_if_j})(g^R_{V_k^0 f_i f_j} - g^L_{V_k^0 f_i f_j}) \\
&\quad \times \Big[2(m_{f_j} - m_{f_i}) \Big(C_{22} + C_{12} \Big)(0, q^2, M_H^2, m_{f_j}^2, m_{f_j}^2, m_{f_i}^2) \\
&\quad + (3m_{f_j} - m_{f_i}) C_2(0, q^2, M_H^2, m_{f_j}^2, m_{f_j}^2, m_{f_i}^2) + m_{f_j} C_0(0, q^2, M_H^2, m_{f_j}^2, m_{f_j}^2, m_{f_i}^2) \Big] \Big\},
\end{aligned}
\tag{26}
$$

$$
F^{\text{Trig}}_{k,R}|_{f_i,f_j} = F^{\text{Trig}}_{k,L}|_{f_i,f_j} (g^L_{V_k^0 \nu_l \bar{\nu}_l} \to g^R_{V_k^0 \nu_l \bar{\nu}_l}). \tag{27}
$$

2.2.2. One-loop box diagrams

We turn our attention to all one-loop box Feynman diagrams contributing to the decay processes. First, one-loop four-point Feynman diagrams having V_i, V_j in the loop (as described in Fig. 6) are performed. The form factors $F^{\text{Box}}_{k,L/R}$ with $k = 1, 2$ are then given by

$$
\begin{aligned}
F^{\text{Box}}_{1,L}|_{V_i,V_j} = \sum_{V_i,V_j} & \frac{eQg_{HV_iV_j}\, g^L_{V_i l \nu_l}\, g^L_{V_j l \nu_l}}{16\pi^2 M_{V_i}^2 M_{V_j}^2} \\
& \times \Big\{ (M_H^2 + M_{V_i}^2 + M_{V_j}^2) \Big[(C_{22} + C_{12})(0, q_{12}, M_H^2, M_{V_i}^2, M_{V_i}^2, M_{V_j}^2) \\
& \qquad + (C_{22} + C_{12})(q_{12}, 0, M_H^2, M_{V_i}^2, M_{V_j}^2, M_{V_j}^2) \Big]
\end{aligned}
$$

$$
\begin{aligned}
&+ (M_H^2 + 3M_{V_i}^2 - M_{V_j}^2)\Big[C_2(0, q_{12}, M_H^2, M_{V_i}^2, M_{V_i}^2, M_{V_j}^2) \\
&\qquad + C_2(q_{12}, 0, M_H^2, M_{V_i}^2, M_{V_j}^2, M_{V_j}^2)\Big] \\
&+ (2M_{V_i}^2 - 2M_{V_j}^2)C_1(q_{12}, 0, M_H^2, M_{V_i}^2, M_{V_j}^2, M_{V_j}^2) \\
&+ 2M_{V_i}^2\Big[C_0(0, q_{12}, M_H^2, M_{V_i}^2, M_{V_i}^2, M_{V_j}^2) + C_0(q_{12}, 0, M_H^2, M_{V_i}^2, M_{V_j}^2, M_{V_j}^2)\Big] \\
&+ m_l^2\Big[(C_{22} + C_{12} + C_2)(0, 0, q_{13}, m_l^2, m_l^2, M_{V_j}^2) \\
&\qquad - (C_{22} + C_{12} + C_2)(0, 0, q_{13}, m_l^2, M_{V_j}^2, M_{V_j}^2)\Big] \\
&+ \Big[m_l^2(M_H^2 + M_{V_i}^2 + M_{V_j}^2) + (2d-4)M_{V_i}^2 M_{V_j}^2\Big] \\
&\times \Big[(D_{33} + D_{23})(0, 0, 0, M_H^2; q_{12}, q_{13}, M_{V_i}^2, m_l^2, M_{V_j}^2, M_{V_j}^2) \\
&\qquad + (D_{33} + D_{23} + D_{13})(0, 0, 0, M_H^2; q_{23}, q_{12}, M_{V_i}^2, M_{V_i}^2, m_l^2, M_{V_j}^2) \\
&\qquad - (D_{33} + D_{23})(0, 0, 0, M_H^2; q_{23}, q_{13}, M_{V_i}^2, m_l^2, m_l^2, M_{V_j}^2)\Big] \\
&+ \Big[m_l^2(M_H^2 + 3M_{V_i}^2 - M_{V_j}^2) + (2d-8)M_{V_i}^2 M_{V_j}^2\Big] \\
&\qquad \times \Big[D_3(0, 0, 0, M_H^2; q_{12}, q_{13}, M_{V_i}^2, m_l^2, M_{V_j}^2, M_{V_j}^2) \\
&\qquad\quad + D_3(0, 0, 0, M_H^2; q_{23}, q_{12}, M_{V_i}^2, M_{V_i}^2, m_l^2, M_{V_j}^2) \\
&\qquad\quad - D_3(0, 0, 0, M_H^2; q_{23}, q_{13}, M_{V_i}^2, m_l^2, m_l^2, M_{V_j}^2)\Big] \\
&+ \Big[2m_l^2(M_{V_i}^2 - M_{V_j}^2) - 4M_{V_i}^2 M_{V_j}^2\Big]D_2(0, 0, 0, M_H^2; q_{12}, q_{13}, M_{V_i}^2, m_l^2, M_{V_j}^2, M_{V_j}^2) \\
&+ 2m_l^2 M_{V_i}^2\Big[D_0(0, 0, 0, M_H^2; q_{12}, q_{13}, M_{V_i}^2, m_l^2, M_{V_j}^2, M_{V_j}^2) \\
&\qquad + D_0(0, 0, 0, M_H^2; q_{23}, q_{12}, M_{V_i}^2, M_{V_i}^2, m_l^2, M_{V_j}^2) \\
&\qquad - D_0(0, 0, 0, M_H^2; q_{23}, q_{13}, M_{V_i}^2, m_l^2, m_l^2, M_{V_j}^2)\Big]\Big\}, \qquad (28)
\end{aligned}
$$

$$F_{1,R}^{\text{Box}}|_{V_i,V_j} = F_{1,L}^{\text{Box}}|_{V_i,V_j}(g_{V_i l\nu_l}^L \to g_{V_i l\nu_l}^R;\ g_{V_j l\nu_l}^L \to g_{V_j l\nu_l}^R), \qquad (29)$$

$$F_{2,L}^{\text{Box}}|_{V_i,V_j} = F_{1,L}^{\text{Box}}|_{V_i,V_j}(\{q_{13}, q_{23}\} \to \{q_{23}, q_{13}\}), \qquad (30)$$

$$F_{2,R}^{\text{Box}}|_{V_i,V_j} = F_{2,L}^{\text{Box}}|_{V_i,V_j}(g_{V_i l\nu_l}^L \to g_{V_i l\nu_l}^R;\ g_{V_j l\nu_l}^L \to g_{V_j l\nu_l}^R). \qquad (31)$$

We find that analytic results for the above form factors are given up to D_{33}-coefficient functions. The reason for that fact can be explained as follows. Although tensor one-loop box integrals with rank $P \geq 4$ appear in each Feynman diagram in Fig. 6, we find that these terms are cancelled out after summing all diagrams. Consequently, the amplitudes are only decomposed up to one-loop box integrals with rank $P = 2$.

We next consider one-loop box diagrams with V_i, S_j in the loop. In order to get the symmetry of $F_{k,L/R}^{\text{Box}}$ which follow the relation

$$F_{1,L/R}^{\text{Box}}|_{V_i,S_j} = F_{2,L/R}^{\text{Box}}|_{V_i,S_j}(\{q_{13}, q_{23}\} \to \{q_{23}, q_{13}\}), \qquad (32)$$

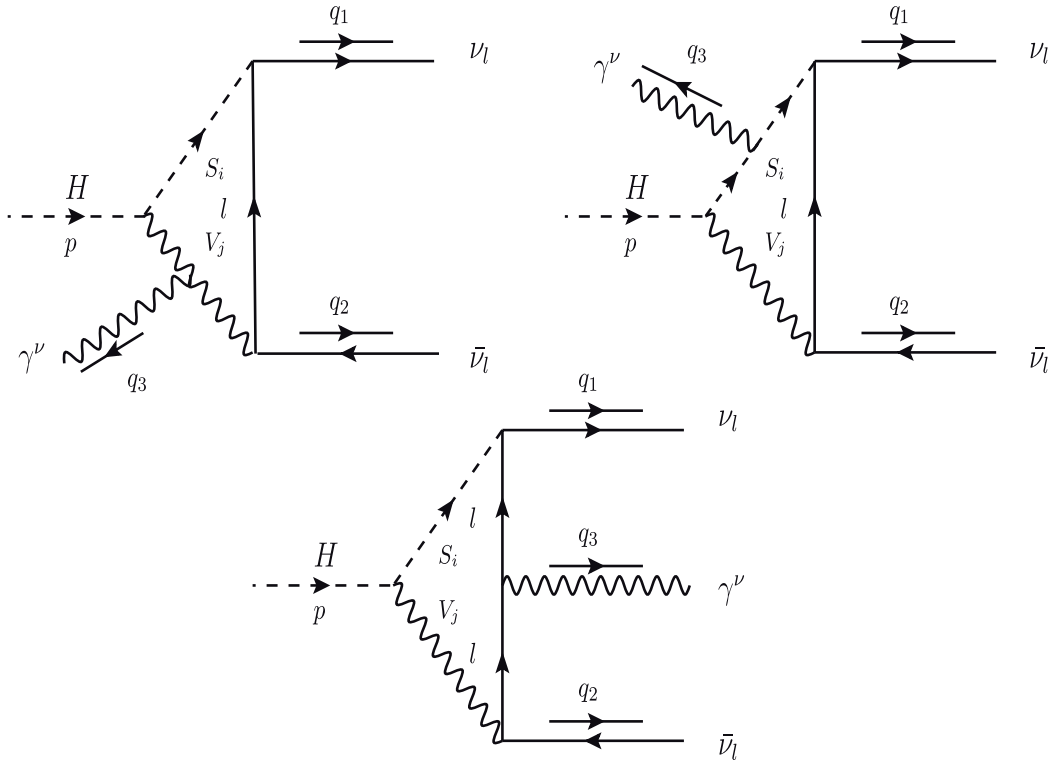

Fig. 7. Feynman box diagrams for $V_{i,j}, S_{i,j}$ in the loop.

we should consider the 6 diagrams shown in Fig. 7 and Fig. 8 together. This is because the coupling of charged scalar $S_i^{\pm}$ to $l\bar{\nu}_l$ (and to $\bar{l}\nu_l$) take different forms (seen Table C.2 for more detail).

The form factors $F^{\text{Box}}_{k,L/R}$ are then presented as follows:

$$
\begin{aligned}
F^{\text{Box}}_{1,L}|_{V_i,S_j} = \sum_{V_i,S_j} \frac{eQm_l\, g_{HV_iS_j}\, g^R_{S_jl\nu_l} g^L_{V_il\nu_l}}{16\pi^2 M^2_{V_i}} \\
\times \Big\{ (M_H^2 - M_{S_j}^2 + M_{V_i}^2)\Big[(D_{33} + D_{23} + D_{13})(0,0,0,M_H^2; q_{23}, q_{12}, M_{V_i}^2, M_{V_i}^2, m_l^2, M_{S_j}^2) \\
- (D_{33} + D_{23} + D_{13})(0,0,0,M_H^2; q_{23}, q_{12}, M_{S_j}^2, M_{S_j}^2, m_l^2, M_{V_i}^2) \\
- (D_{33} + D_{23})(0,0,0,M_H^2; q_{12}, q_{13}, M_{V_i}^2, m_l^2, M_{S_j}^2, M_{S_j}^2) \\
+ (D_{33} + D_{23})(0,0,0,M_H^2; q_{12}, q_{13}, M_{S_j}^2, m_l^2, M_{V_i}^2, M_{V_i}^2) \\
- (D_{33} + D_{23})(0,0,0,M_H^2; q_{23}, q_{13}, M_{V_i}^2, m_l^2, m_l^2, M_{S_j}^2) \\
- (D_{33} + D_{23})(0,0,0,M_H^2; q_{23}, q_{13}, M_{S_j}^2, m_l^2, m_l^2, M_{V_i}^2) \Big] \\
+ (M_H^2 - M_{S_j}^2 + 3M_{V_i}^2)\Big[D_3(0,0,0,M_H^2; q_{23}, q_{12}, M_{V_i}^2, M_{V_i}^2, m_l^2, M_{S_j}^2) \\
- D_3(0,0,0,M_H^2; q_{12}, q_{13}, M_{V_i}^2, m_l^2, M_{S_j}^2, M_{S_j}^2) \\
- D_3(0,0,0,M_H^2; q_{23}, q_{13}, M_{V_i}^2, m_l^2, m_l^2, M_{S_j}^2) \Big]
\end{aligned}
$$

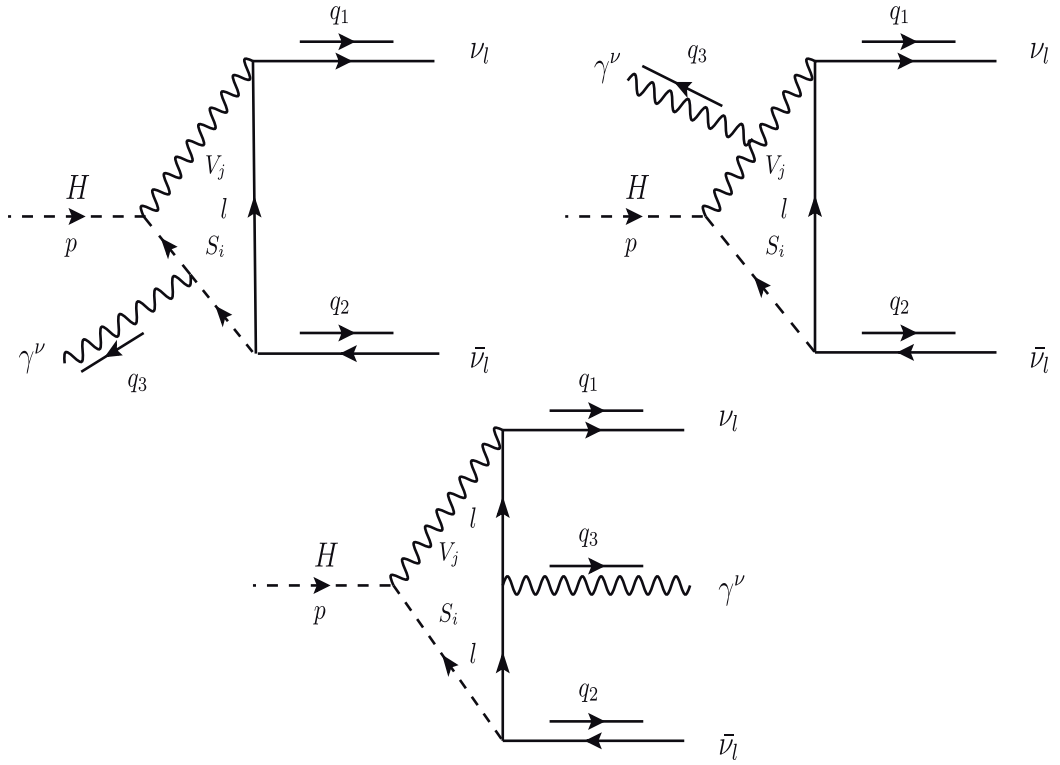

Fig. 8. Feynman box diagrams for $V_{i,j}, S_{i,j}$ in the loop.

$$
\begin{aligned}
&+ (M_H^2 - M_{S_j}^2 - M_{V_i}^2)\Big[D_3(0,0,0,M_H^2;q_{12},q_{13},M_{S_j}^2,m_l^2,M_{V_i}^2,M_{V_i}^2) \\
&\qquad - D_3(0,0,0,M_H^2;q_{23},q_{12},M_{S_j}^2,M_{S_j}^2,m_l^2,M_{V_i}^2) \\
&\qquad - D_3(0,0,0,M_H^2;q_{23},q_{13},M_{S_j}^2,m_l^2,m_l^2,M_{V_i}^2)\Big] \\
&+ 2M_{V_i}^2\Big[D_0(0,0,0,M_H^2;q_{23},q_{12},M_{V_i}^2,M_{V_i}^2,m_l^2,M_{S_j}^2) \\
&\qquad - D_0(0,0,0,M_H^2;q_{23},q_{13},M_{V_i}^2,m_l^2,m_l^2,M_{S_j}^2) \\
&\qquad - (D_2+D_0)(0,0,0,M_H^2;q_{12},q_{13},M_{V_i}^2,m_l^2,M_{S_j}^2,M_{S_j}^2) \\
&\qquad - D_2(0,0,0,M_H^2;q_{12},q_{13},M_{S_j}^2,m_l^2,M_{V_i}^2,M_{V_i}^2)\Big] \\
&- 3\Big[(C_{22}+C_{12}+C_2)(0,0,q_{13},m_l^2,m_l^2,M_{S_j}^2) \\
&\qquad + (C_{22}+C_{12}+C_2)(0,0,q_{13},m_l^2,M_{S_j}^2,M_{S_j}^2)\Big] \\
&+ (C_{22}+C_{12}+C_2)(0,0,q_{13},m_l^2,m_l^2,M_{V_i}^2) \\
&- (C_{22}+C_{12}+C_2)(0,0,q_{13},m_l^2,M_{V_i}^2,M_{V_i}^2)\Big\},
\end{aligned}
\tag{33}
$$

$$
F_{1,R}^{\text{Box}}|_{V_i,S_j} = F_{1,L}^{\text{Box}}|_{V_i,S_j}(g_{S_j l\nu_l}^R \to g_{S_j l\nu_l}^L; g_{V_i l\nu_l}^L \to g_{V_i l\nu_l}^R), \tag{34}
$$

$$
F_{2,R}^{\text{Box}}|_{V_i,S_j} = F_{2,L}^{\text{Box}}|_{V_i,S_j}(g_{S_j l\nu_l}^R \to g_{S_j l\nu_l}^L; g_{V_i l\nu_l}^L \to g_{V_i l\nu_l}^R). \tag{35}
$$

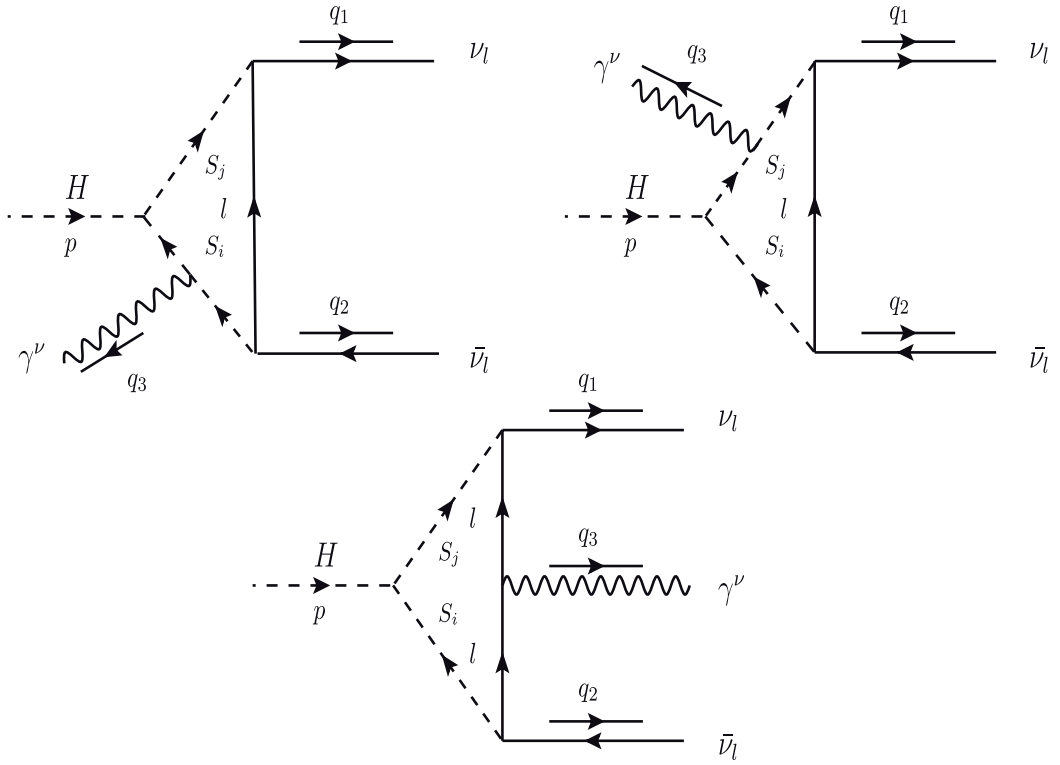

Fig. 9. Feynman box diagrams for $S_{i,j}$ in the loop.

In the SM limit, we observe that these contributions are much smaller than other contributions because of the appearance of the factor m_l/M_{V_i} in Eq. (33). This means that we can only take the τ-lepton contributions for these form factors. However, in many BSMs, where new heavy charged leptons with $m_{E_l} \gg m_l$ appear in the loop, these contributions may be significant. For this case, the form factors are obtained directly by replacing l by E_l. We finally end up with the contributions of one-loop box diagrams with charged scalar bosons S_i, S_j in the loop (see Fig. 9). The corresponding form factors read:

$$\begin{aligned} F_{1,L}^{\text{Box}}|_{S_i,S_j} = &-\sum_{S_i,S_j} \frac{eQg_{HS_iS_j}\, g^R_{S_i l\nu_l}\, g^R_{S_j l\nu_l}}{8\pi^2} \\ &\times \Big\{ (D_{33}+D_{23}+D_3)(0,0,0,M_H^2;q_{12},q_{13},M_{S_i}^2,m_l^2,M_{S_j}^2,M_{S_j}^2) \\ &+ (D_{33}+D_{23}+D_{13}+D_3)(0,0,0,M_H^2;q_{23},q_{12},M_{S_i}^2,M_{S_i}^2,m_l^2,M_{S_j}^2) \\ &+ (D_{33}+D_{23}+D_3)(0,0,0,M_H^2;q_{23},q_{13},M_{S_i}^2,m_l^2,m_l^2,M_{S_j}^2) \Big\}, \end{aligned} \tag{36}$$

$$F_{1,R}^{\text{Box}}|_{S_i,S_j} = F_{1,L}^{\text{Box}}|_{S_i,S_j}(g^R_{S_i l\nu_l} \to g^L_{S_i l\nu_l};\ g^R_{S_j l\nu_l} \to g^L_{S_j l\nu_l}), \tag{37}$$

$$F_{2,L}^{\text{Box}}|_{S_i,S_j} = F_{1,L}^{\text{Box}}|_{S_i,S_j}(\{q_{13},q_{23}\} \to \{q_{23},q_{13}\}), \tag{38}$$

$$F_{2,R}^{\text{Box}}|_{S_i,S_j} = F_{2,L}^{\text{Box}}|_{S_i,S_j}(g^R_{S_i l\nu_l} \to g^L_{S_i l\nu_l};\ g^R_{S_j l\nu_l} \to g^L_{S_j l\nu_l}). \tag{39}$$

In Appendix A, we prove analytically and check numerically the UV finiteness of the results. We find that the UV-divergent parts of all the above form factors come from all B-functions and the C_{22}-, C_{12}- and C_2-functions, while C_0-, D_0- D_i- and D_{ij}-functions are UV-finite. We prove that the sum of all B-functions gives a UV-finite result (see Appendix A for more detail). Furthermore, C_2-functions are reduced to two B_0-functions and their UV-divergent parts are cancelled out. Lastly, the remaining functions C_{22} and C_{12} always appear together as the form of $C_{22} + C_{12}$ in all the form factors. They are also UV-finite in the limit of $d \to 4$.

All the above form factors are also checked numerically by verifying the UV finiteness of the results. We find that the results are in good stability when varying UV cutoff parameters. We refer numerical results for this check in Appendix A.

Having the correct form factors for the decay processes, the decay width is given by [36]:

$$\frac{d\Gamma}{dq_{12}\,dq_{13}} = \frac{q_{12}}{512\pi^3 M_H^3}\Big[q_{13}^2(|F_{1,R}|^2 + |F_{2,R}|^2) + q_{23}^2(|F_{1,L}|^2 + |F_{2,L}|^2)\Big]. \tag{40}$$

Taking the above integrand over q_{12} and q_{13} in the region $0 \le q_{12} \le M_H^2$ and $0 \le q_{13} \le M_H^2 - q_{12}$, one gets the total decay width. In the next subsection, we show a typical example where we apply the analytic results for $H \to \nu_l \bar{\nu}_l \gamma$ in SM. Phenomenological results for these decay channels is also studied using updated parameters at the LHC.

2.2.3. *Standard model case*

In this case, we have $V_i, V_j \to W^+, W^-$, $V_k^0 \to Z$. All couplings are replaced by $g_{HV_iV_j} = eM_W/s_W$, $g_{V_k^0V_iV_j} = e\ c_W/s_W$, $g_{V_k^0AV_iV_j} = e^2\ c_W/s_W$, $g^L_{V_k^0\nu_l\nu_l} = e/(2s_Wc_W)$, $g^R_{V_k^0\nu_l\nu_l} = 0$, $g^L_{Hf_if_j} = g^R_{Hf_if_j} = e\ m_f/(2s_W\ M_W)$, $g^L_{V_k^0f_if_j} = e(T_3^f - Q_f\ s_W^2)/(s_W\ c_W)$, $g^R_{V_k^0f_if_j} = -eQ_fs_W/c_W$, $g^L_{V_il\nu_l} = e/(\sqrt{2}\ s_W)$ and $g^R_{V_il\nu_l} = 0$. Analytic results for the case of $m_l \to 0$ are presented as follows:

$$\begin{aligned}
F_{1,L}^{\text{Trig, SM}}|_{W,W} = {} & \frac{\alpha^2}{4M_W^3 s_W^3 (q^2 - M_Z^2 + i\Gamma_Z M_Z)} \\
& \times \Big\{\Big[M_H^2(2B_{111} + 3B_{11} + B_1) + 2B_{00} + 4B_{001}\Big](M_H^2, M_W^2, M_W^2) \\
& + \Big[4M_H^2M_W^2 - 2M_H^2q^2 + 8(d-1)M_W^4 - 4M_W^2q^2\Big] \\
& \qquad \times \Big[C_{22} + C_{12} + C_2\Big](0, q^2, M_H^2, M_W^2, M_W^2, M_W^2) \\
& + 4M_W^2(4M_W^2 - q^2)C_0(0, q^2, M_H^2, M_W^2, M_W^2, M_W^2)\Big\},
\end{aligned} \tag{41}$$

$$\begin{aligned}
F_{1,L}^{\text{Trig, SM}}|_{f,f} = {} & -\frac{\alpha^2 m_f^2 N_C^f Q_f}{2c_W^2 s_W^3 M_W (q^2 - M_Z^2 + i\Gamma_Z M_Z)}\left(2Q_f s_W^2 - T_3^f\right) \\
& \times \Big\{C_0(0, q^2, M_H^2, m_f^2, m_f^2, m_f^2) + 4\Big[C_{22} + C_{12} + C_2\Big](0, q^2, M_H^2, m_f^2, m_f^2, m_f^2)\Big\}.
\end{aligned} \tag{42}$$

We also have $F_{k,R}^{\text{Trig, SM}}|_{W,W} = F_{k,R}^{\text{Trig, SM}}|_{f,f} = 0$ for $k = 1, 2$ due to the fact that all couplings $g_{\dots}^{R}$ are absent from the SM. For one-loop box diagrams, the form factors read

$$\begin{aligned}
F_{1,L}^{\text{Box, SM}}|_{W,W} = \frac{\alpha^2}{2M_W^3 s_W^3}\Big\{ & (M_H^2 + 2M_W^2)\Big[(C_{22} + C_{12} + C_2)(0, q_{12}, M_H^2, M_W^2, M_W^2, M_W^2) \\
& + (C_{22} + C_{12} + C_2)(q_{12}, 0, M_H^2, M_W^2, M_W^2, M_W^2)\Big] \\
& + 2(d-2)M_W^4\Big[(D_{33} + D_{23})(0, 0, 0, M_H^2; q_{12}, q_{13}; M_W^2, 0, M_W^2, M_W^2) \\
& + (D_{33} + D_{23})(0, 0, 0, M_H^2; q_{23}, q_{13}; M_W^2, 0, 0, M_W^2) \\
& + (D_{33} + D_{23} + D_{13})(0, 0, 0, M_H^2; q_{23}, q_{12}; M_W^2, M_W^2, 0, M_W^2)\Big] \\
& + 2(d-4)M_W^4\Big[D_3(0, 0, 0, M_H^2; q_{12}, q_{13}; M_W^2, 0, M_W^2, M_W^2) \\
& + D_3(0, 0, 0, M_H^2; q_{23}, q_{12}; M_W^2, M_W^2, 0, M_W^2) \\
& + D_3(0, 0, 0, M_H^2; q_{23}, q_{13}; M_W^2, 0, 0, M_W^2)\Big] \\
& + 4M_W^2\Big[C_0(0, q_{12}, M_H^2, M_W^2, M_W^2, M_W^2) \\
& - M_W^2 D_2(0, 0, 0, M_H^2; q_{12}, q_{13}; M_W^2, 0, M_W^2, M_W^2)\Big]\Big\},
\end{aligned} \tag{43}$$

$$F_{2,L}^{\text{Box, SM}}|_{W,W} = F_{1,L}^{\text{Box, SM}}|_{W,W}\,(\{q_{13}, q_{23}\} \to \{q_{23}, q_{13}\})\,, \tag{44}$$

$$F_{1,R}^{\text{Box, SM}}|_{W,W} = F_{2,R}^{\text{Box, SM}}|_{W,W} = 0. \tag{45}$$

For phenomenological results, we use following input parameters: $M_Z = 91.1876$ GeV, $\Gamma_Z = 2.4952$ GeV, $M_W = 80.379$ GeV, $M_H = 125.1$ GeV, $m_\tau = 1.77686$ GeV, $m_t = 172.76$ GeV, $m_b = 4.18$ GeV, $m_s = 0.93$ GeV and $m_c = 1.27$ GeV. We first confirm the previous result in Ref. [13] in which the decay width is computed in α-scheme, or $\alpha = 1/137.035999084$. By working in this scheme, the decay width (for $l = e$) is obtained as $\Gamma_{H\to\nu_e\bar{\nu}_e\gamma} = 0.480414$ KeV. This value gives a good agreement with the result in Ref. [13].

At the LHC, the decay processes are involved two kind of events: (i) in the case where a photon is undetected, we then have Higgs decay to invisible particles; (ii) for a detected photon, we observe the Higgs decay to a photon plus missing energy. The former events provide important information for controlling the SM background for $H \to \gamma\gamma$ and $H \to Z\gamma$ where Z may decay to undetected leptons, etc. The latter events are interesting for searching dark matter at the LHC. Both events are examined in this paper using the present parameters at the LHC. In this computation, we work in the G_F-scheme in which α is evaluated from $G_F = 1.1663787 \times 10^{-5}$ GeV^{-2}. The result reads

$$\alpha^{-1} = \frac{\pi}{\sqrt{2}G_F M_W^2 s_W^2} = 132.184. \tag{46}$$

The following new results for decay widths are obtained:

$$\Gamma_{H\to\nu_l\bar{\nu}_l\gamma}^{\text{Trig}} = 0.536234\ \text{KeV}, \tag{47}$$

$$\Gamma_{H\to\nu_l\bar{\nu}_l\gamma}^{\text{Tot}} = 0.554933\ \text{KeV}. \tag{48}$$

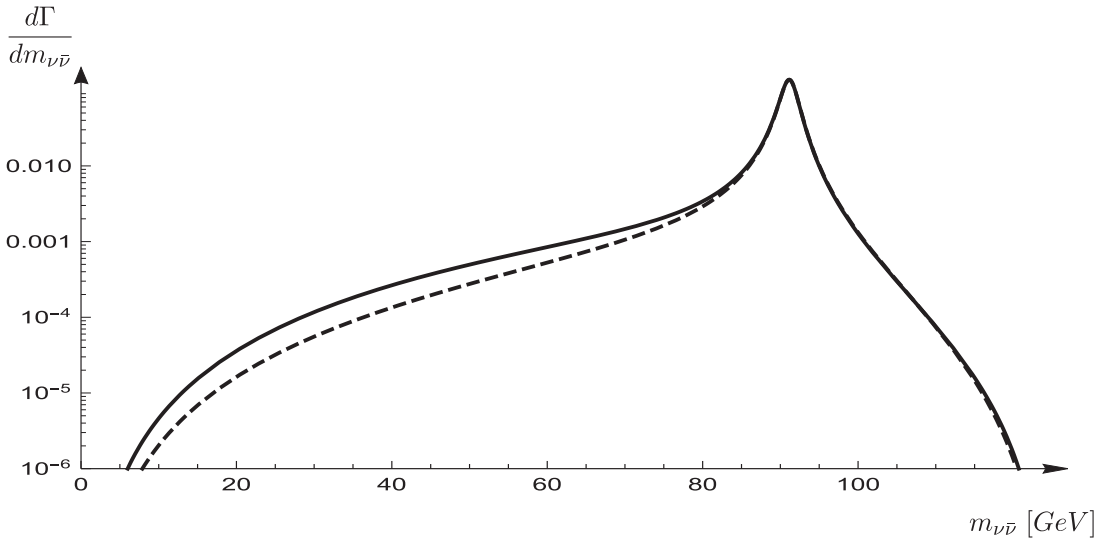

Fig. 10. Differential decay width is plotted as function of invariant mass of $m_{\nu_l\bar{\nu}_l}$.

Table 1. Decay widths in the case of photon that can be tested.

Γ [KeV]/$E_\gamma^{\rm cut}$ [GeV]	5	30	50
$\Gamma^{\rm Trig}_{H\to\gamma\nu_l\bar{\nu}_l}$	0.536232	0.188952	0.00529925
$\Gamma^{\rm Total}_{H\to\gamma\nu_l\bar{\nu}_l}$	0.554931	0.20927	0.00993683

We realize that the attributions of $|F^{\rm Box}_{k/L(R)}|^2$ are much smaller than those of the other terms. The differential decay width is also plotted as function of the invariant mass $m_{\nu_l\bar{\nu}_l}$ (or $m_{\nu_l\bar{\nu}_l} = \sqrt{q_{12}}$). The distribution is defined in the form of

$$\frac{d\Gamma}{dm_{\nu_l\bar{\nu}_l}} = \frac{m^3_{\nu_l\bar{\nu}_l}}{512\pi^3 M_H^3} \int_0^{M_H^2-2m^2_{\nu_l\bar{\nu}_l}} dq_{13}\Big[q_{13}^2(|F_{1,R}|^2+|F_{2,R}|^2)+q_{23}^2(|F_{1,L}|^2+|F_{2,L}|^2)\Big]. \quad (49)$$

The distribution is shown in Fig. 10. The solid line shows the total contributions, while the dashed line represents the interference between three-point diagrams and box diagrams. We observe a peak of $Z^* \to \nu_l\bar{\nu}_l$ which is around M_Z. In the region $m_{\nu\bar{\nu}} \le M_Z$, the contributions of box diagrams are visible, while they give a small contribution beyond the peak. We are also interested in the case of a photon that can be tested at the colliders. In this case, one should apply the energy cuts for the final photon. The results are shown with different cuts for photons in Table 1. The results are important and should be taken into account at the HL-LHC and future colliders.

We note that all numerical results shown in this subsection are for a family of neutrinos in the final state. For all neutrinos, we multiply by a factor 3 for all above results.

2.2.4. Two Higgs Doublet Model case

We next consider the case of the THDM [18]. We devote Appendix B to reviewing the model, and derive all couplings involving the decay channels. Applying the calculation to this model, we have $V_i, V_j \to W^+, W^-$, $V_k^0 \to Z$ and $S_i, S_j \to H^\pm$. All related couplings $g_{HV_iV_j} = (2M_W^2/v)s_{(\beta-\alpha)}$, $g_{HS_iS_j} = -(1/v)\Big[(2\mu^2 - 2M_{H^\pm} - M^2_{H_1^0})s_{(\beta-\alpha)} + 2(\mu^2 - M^2_{H_1^0})\cot 2\beta\ c_{(\beta-\alpha)}\Big]$,

$g_{HV_iS_j} = (M_W/v)c_{(\beta-\alpha)}$, $g_{AS_iS_j} = (2M_W/v)s_W = e$, $g_{V_k^0S_iS_j} = (M_Z/v)c_{2W}$, $g^L_{Hf_if_j} = g^R_{Hf_if_j} = \lambda^L_\tau = \lambda^R_\tau$, $g^L_{S_i\tau\nu_\tau} = Y_\tau$ and $g^R_{S_i\tau\nu_\tau} = Y_{\nu_\tau}$. Putting these couplings and masses of charged Higgs in to the above results, we can derive one-loop formulas for the form factors of the decay processes in THDM. For phenomenological analysis, one should combine this calculation with the current measurements at the LHC, for examples the data on $H \to \gamma\gamma$, $Z\gamma$, $H \to f\bar{f}$, etc. These topics are beyond the scope of the current paper. We will devote our future paper to the phenomenological analysis of the decay channels in THDM and many BSMs.

3. Conclusions

We have presented analytic formulas for all possible one-loop contributions to the SM-like Higgs decay $H \to \nu_l\bar{\nu}_l\gamma$ that are valid in many BSMs. Additional vector bosons, charged fermions and charged (and also neutral) scalar particles exchanging in the loop diagrams have been considered in this computation. We also conclude that the evaluations can be extended directly for general numbers of the extra neutrinos in final states. Analytic results are expressed in a general form, written in terms of Passarino–Veltman scalar functions that can be evaluated numerically using `LoopTools`. The computations have been checked numerically by verifying UV finiteness of the results. We find that the results are in good stability when varying UV cutoff parameters. We then apply the results to the SM and the decay widths are generated and cross-checked with previous computations. All physical results for the decay channels within SM have been studied with the present input parameters at the LHC. Furthermore, the calculation has also been applied successfully to THDM. As the outlook beyond this work, we plan to apply the computation for the phenomenological analysis in many BSMs.

Acknowledgements

This research is funded by Vietnam National Foundation for Science and Technology Development (NAFOSTED) under the grant number 103.01-2019.387.

Funding

Open Access funding: SCOAP[3].

Appendix A. Checks for the calculations

We check for the UV finiteness of the results in order to understand how the UV cutoff ($C_{UV} = 1/\varepsilon$) parameter can be cancelled out from the final results. We take the results in Eq. (18) as an example. In the SM $V_k^0 = Z$ and $V_i = V_j = W^\pm$, we then have the relation $g_{ZAV_iV_i} = eQg_{ZV_iV_i}$ (A represents the photon) because of the condition that the gauge symmetry breaks to quantum electrodynamic (QED) at the final stage. In many BSMs, there may exist a relation between the couplings of photons and other gauge bosons:

$$g_{V_k^0AV_iV_j} = eQg_{V_k^0V_iV_j}. \tag{A.1}$$

We first reduce all PV-functions in (18) to scalar one-loop integrals as follows:

$$B_1(M_H^2, M_{V_j}^2, M_{V_i}^2) = \\ = \frac{1}{2M_H^2}\Big[A_0(M_{V_j}^2) - A_0(M_{V_i}^2) + (M_{V_i}^2 - M_{V_j}^2 - M_H^2)B_0(M_H^2, M_{V_j}^2, M_{V_i}^2)\Big], \tag{A.2}$$

$$B_{00}(M_H^2, M_{V_j}^2, M_{V_i}^2) = \frac{1}{4M_H^2(d-1)} \times \Big\{(M_H^2 + M_{V_j}^2 - M_{V_i}^2)A_0(M_{V_j}^2) + (M_H^2 - M_{V_j}^2 + M_{V_i}^2)A_0(M_{V_i}^2) - \Big[M_H^4 - 2M_H^2(M_{V_j}^2 + M_{V_i}^2) + (M_{V_j}^2 - M_{V_i}^2)^2\Big]B_0(M_H^2, M_{V_j}^2, M_{V_i}^2)\Big\}, \tag{A.3}$$

$$B_{11}(M_H^2, M_{V_j}^2, M_{V_i}^2) = \frac{1}{4M_H^4(d-1)} \times \Big\{\Big[d(M_H^2 + M_{V_j}^2 - M_{V_i}^2)^2 - 4M_H^2 M_{V_j}^2\Big]B_0(M_H^2, M_{V_j}^2, M_{V_i}^2) - d(M_H^2 + M_{V_j}^2 - M_{V_i}^2)A_0(M_{V_j}^2) + \Big[(3d-4)M_H^2 + d(M_{V_j}^2 - M_{V_i}^2)\Big]A_0(M_{V_i}^2)\Big\}, \tag{A.4}$$

$$B_{001}(M_H^2, M_{V_j}^2, M_{V_i}^2) = \frac{1}{8M_H^4 d(d-1)}\Big\{d\Big[M_H^6 - M_H^4(M_{V_j}^2 + 3M_{V_i}^2) - M_H^2(M_{V_j}^4 + 2M_{V_j}^2 M_{V_i}^2 - 3M_{V_i}^4) + (M_{V_j}^2 - M_{V_i}^2)^3\Big]B_0(M_H^2, M_{V_j}^2, M_{V_i}^2) - \Big\{4M_H^2 M_{V_j}^2 + d\Big[M_H^4 - 2M_H^2(M_{V_j}^2 + M_{V_i}^2) + (M_{V_j}^2 - M_{V_i}^2)^2\Big]\Big\}A_0(M_{V_j}^2) + \Big\{4M_H^2 M_{V_i}^2 - d\Big[M_H^4 + 4M_H^2 M_{V_i}^2 - (M_{V_j}^2 - M_{V_i}^2)^2\Big]\Big\}A_0(M_{V_i}^2)\Big\}, \tag{A.5}$$

$$B_{111}(M_H^2, M_{V_j}^2, M_{V_i}^2) = \frac{1}{8M_H^6 d(1-d)} \times \Big\{(M_H^2 + M_{V_j}^2 - M_{V_i}^2)\Big\{d(d+2)\Big[M_H^4 - 2M_H^2 M_{V_i}^2 + (M_{V_j}^2 - M_{V_i}^2)^2\Big] + 2d(d-4)M_H^2 M_{V_j}^2\Big\}B_0(M_H^2, M_{V_j}^2, M_{V_i}^2) - \Big\{d^2(M_H^2 + M_{V_j}^2 - M_{V_i}^2)^2 + 8M_H^2 M_{V_j}^2 + 2d\Big[M_H^4 - 2M_H^2(M_{V_j}^2 + M_{V_i}^2) + (M_{V_j}^2 - M_{V_i}^2)^2\Big]\Big\}A_0(M_{V_j}^2) + \Big\{8M_H^2 M_{V_i}^2 + d^2\Big[3M_H^4 + (2M_H^2 + M_{V_j}^2 - M_{V_i}^2)^2\Big] - 2d\Big[5M_H^4 + 2M_H^2(M_{V_j}^2 + M_{V_i}^2) - (M_{V_j}^2 - M_{V_i}^2)^2\Big]\Big\}A_0(M_{V_i}^2)\Big\}. \tag{A.6}$$

For C-functions, we also have

$$C_{22}(0, q^2, M_H^2, M_{V_j}^2, M_{V_j}^2, M_{V_i}^2) = = \frac{1}{2M_H^2 q^2(M_H^2 - q^2)}\Big\{M_H^2(M_{V_j}^2 - M_{V_i}^2 + q^2)B_0(q^2, M_{V_j}^2, M_{V_i}^2)$$

$$+ q^2(M_{V_i}^2 - M_{V_j}^2 - M_H^2)B_0(M_H^2, M_{V_j}^2, M_{V_i}^2) + (q^2 - M_H^2)\Big[A_0(M_{V_j}^2) - A_0(M_{V_i}^2)\Big]\Big\}, \tag{A.7}$$

$$C_{12}(0, q^2, M_H^2, M_{V_j}^2, M_{V_j}^2, M_{V_i}^2) = \frac{1}{2q^2(M_H^2 - q^2)^2(d-2)}$$
$$\times \Big\{\Big[d\, q^2(M_{V_j}^2 - M_{V_i}^2 - q^2) + 4q^4 - (d-2)M_H^2(M_{V_j}^2 - M_{V_i}^2 - q^2)\Big]B_0(q^2, M_{V_j}^2, M_{V_i}^2)$$
$$+ 2q^2(M_{V_i}^2 - M_{V_j}^2 - M_H^2)B_0(M_H^2, M_{V_j}^2, M_{V_i}^2) + (d-2)(M_H^2 - q^2)\Big[A_0(M_{V_j}^2) - A_0(M_{V_i}^2)\Big]$$
$$+ 4M_{V_j}^2 q^2(q^2 - M_H^2)C_0(0, q^2, M_H^2, M_{V_j}^2, M_{V_j}, M_{V_i}^2)\Big\}, \tag{A.8}$$

$$C_2(0, q^2, M_H^2, M_{V_j}^2, M_{V_j}^2, M_{V_i}^2) = \frac{1}{M_H^2 - q^2}\Big[B_0(M_H^2, M_{V_j}^2, M_{V_i}^2) - B_0(q^2, M_{V_j}^2, M_{V_i}^2)\Big]. \tag{A.9}$$

Finally, we present the results in terms of A_0, B_0 and C_0. We know that C_0 functions are UV-finite, while UV-divergent parts of A_0 and B_0 are proportional to $C_{UV} = 1/\varepsilon$ in the limit of $\varepsilon \to 0$ [34] (or $d \to 4$). We find that the sum of all coefficients of C_{UV} will be 0 in the limit of $d \to 4$. As a result, the form factors are UV-finite. In the SM, using the above reduction formulas, the results in Eq. (41) become

$$F_{1,L}^{\text{Trig, SM}}|_{W,W} = \frac{\alpha^2}{2M_W^3 s_W^3(d-2)(M_H^2 - q^2)^2(q^2 - M_Z^2 + i\Gamma_Z M_Z)}$$
$$\times \Big\{\Big[M_H^2(2M_W^2 - q^2) + 4M_W^4(d-1) - 2M_W^2 q^2\Big]$$
$$\times \Big[\Big(M_H^2(d-4) + (2-d)q^2\Big)B_0(M_H^2, M_W^2, M_W^2) + 2q^2 B_0(q^2, M_W^2, M_W^2)\Big]$$
$$+ 4M_W^2(M_H^2 - q^2)\Big[2M_W^2(M_H^2 - q^2)(2d-5) - 4M_W^4(d-1)$$
$$+ q^4(d-2) - M_H^2 q^2(d-3)\Big]C_0(0, q^2, M_H^2, M_W^2, M_W^2, M_W^2)\Big\}. \tag{A.10}$$

In the limit of $d \to 4$, we observe that the term

$$-2q^2 B_0(M_H^2, M_W^2, M_W^2) + 2q^2 B_0(q^2, M_W^2, M_W^2) \to \text{UV-finite}. \tag{A.11}$$

Furthermore, in all other form factors the UV-divergent parts may come from C_2, C_{22} and C_{12}. From the reduction formula (A.9), we verify that C_2 is UV finite when $d \to 4$. The remaining functions are also UV finite. Taking C_{22} as an example, we have

$$\sum_{V_i V_j} C_{22}(0, q^2, M_H^2, M_{V_j}^2, M_{V_j}^2, M_{V_i}^2) =$$
$$= \frac{1}{M_H^2 q^2(M_H^2 - q^2)}\Big\{M_H^2 q^2 B_0(q^2, M_{V_j}^2, M_{V_i}^2) - q^2 M_H^2 B_0(M_H^2, M_{V_j}^2, M_{V_i}^2)\Big\}. \tag{A.12}$$

When $d \to 4$, the above term will be UV-finite. Since D-functions are also UV-finite. Therefore, we conclude that all the form factors are also UV-finite in the limit od $d \to 4$.

Table A.1. Numerical checks for $F_{1L}^{\text{Trig}}|_{WW}$.

Diagrams/(C_{UV}, μ^2)	$(0, 1)$	$(10^5, 10^7)$
1st	$5.684478386592405 \times 10^{-8}$ $+ 7.556282593901243 \times 10^{-8}\, i$	-0.0004193697635384515 $-0.0005574612531042949\, i$
2nd	$5.684478386592405 \times 10^{-8}$ $+ 7.556282593901243 \times 10^{-8}\, i$	-0.0004193697635384515 $-0.0005574612531042948\, i$
3rd	$-6.951714952517838 \times 10^{-8}$ $-9.24079908850924 \times 10^{-8}\, i$	0.00083878369949511 $+ 0.0011149812238695827\, i$
Sum	$4.417241820666968 \times 10^{-8}$ $+5.871766099293248 \times 10^{-8}\, i$	$4.417241820666968 \times 10^{-8}$ $+5.871766099293248 \times 10^{-8}\, i$

Table A.2. Numerical checks for $F_{1L}^{\text{Box}}|_{WW}$.

Diagrams/(C_{UV}, μ^2)	$(0, 1)$	$(10^5, 10^7)$
1st	$-3.114167099931247 \times 10^{-10}$	$-3.114167099931247 \times 10^{-10}$
2nd	$6.440660243424821 \times 10^{-10}$	$6.440660243424821 \times 10^{-10}$
3rd	$-9.02406987251144 \times 10^{-11}$	$-9.02406987251144 \times 10^{-11}$
Sum	$2.424086156242413 \times 10^{-10}$	$2.424086156242413 \times 10^{-10}$

Numerical checks for the computations are performed for all the above form factors. The results must be independent of UV cutoff and μ^2 parameters. To demonstrate, we take the form factors $F_{1L}^{\text{Trig}}|_{WW}$ and $F_{1L}^{\text{Box}}|_{WW}$, which appear as high rank tensor one-loop integrals in the amplitude, as typical examples. Numerical results are presented at an arbitrary sampling point in the physical region. (see Tables A.1, A.2 for more detail).

Appendix B. Review of the Two Higgs Doublet Model

We review briefly the THDM which is broken softly Z_2-symmetry. We base this review on Ref. [18]. There are two scalar doublets Φ_1, Φ_2 with hypercharge $Y = 1/2$. Parts of the Lagrangian which are different from that of SM are written as

$$\mathcal{L} = \mathcal{L}_K + \mathcal{L}_Y - V(\Phi_1, \Phi_2), \tag{B.1}$$

where $\mathcal{L}_K$ is the kinematic term, $\mathcal{L}_Y$ is for the Yukawa part, and $V(\Phi_1, \Phi_2)$ is the Higgs potential. The kinematic term is given as

$$\mathcal{L}_K = \sum_{k=1}^{2} \left(D_\mu \Phi_k\right)^\dagger \left(D^\mu \Phi_k\right), \tag{B.2}$$

with $D_\mu = \partial_\mu - igT^a W_\mu^a - i(g'/2)B_\mu$. The Higgs potential which is broken Z_2-symmetry is expressed as

$$V(\Phi_1, \Phi_2) = \frac{1}{2}m_{11}^2 \Phi_1^\dagger \Phi_1 - m_{12}^2(\Phi_1^\dagger \Phi_2 + \Phi_2^\dagger \Phi_1) + \frac{1}{2}m_{22}^2 \Phi_2^\dagger \Phi_2 + \frac{\lambda_1}{2}\left(\Phi_1^\dagger \Phi_1\right)^2 + \frac{\lambda_2}{2}\left(\Phi_2^\dagger \Phi_2\right)^2$$

$$+\lambda_3\left(\Phi_1^\dagger\Phi_1\right)\left(\Phi_2^\dagger\Phi_2\right)+\lambda_4\left(\Phi_1^\dagger\Phi_2\right)\left(\Phi_2^\dagger\Phi_1\right)+\frac{\lambda_5}{2}\left[\left(\Phi_1^\dagger\Phi_2\right)^2+\left(\Phi_1^\dagger\Phi_2\right)^2\right] \tag{B.3}$$

Here m_{12}^2 plays the role of the soft broken scale of the Z_2-symmetry. The two scalar doublet fields can be parameterized as follows:

$$\Phi_1=\begin{pmatrix}\phi_1^+\\ \dfrac{v_1+\eta_1+i\xi_1}{\sqrt{2}}\end{pmatrix},\quad \Phi_2=\begin{pmatrix}\phi_2^+\\ \dfrac{v_2+\eta_2+i\xi_2}{\sqrt{2}}\end{pmatrix}. \tag{B.4}$$

From the stationary conditions for the Higgs potential, we get

$$m_{11}^2-\mu^2\frac{v_2^2}{v^2}+\frac{\lambda_1}{2}v_1^2+\frac{\lambda_{345}}{2}v_2^2=0, \tag{B.5}$$

$$m_{22}^2-\mu^2\frac{v_1^2}{v^2}+\frac{\lambda_2}{2}v_2^2+\frac{\lambda_{345}}{2}v_1^2=0, \tag{B.6}$$

where $v^2=v_1^2+v_2^2$ is fixed at the electroweak scale $v=(\sqrt{2}G_F)^{-1/2}=246$ GeV and $\mu^2=(v^2/v_1v_2)m_{12}^2$. The mixing angle is defined as $t_\beta=\tan\beta=v_2/v_1$, $\lambda_{345}=\lambda_3+\lambda_4+\lambda_5$. The mass terms of the Higgs potential $V_{\rm mass}$ can be expressed as:

$$\begin{aligned}V_{\rm mass}=&(\phi_1^+,\phi_2^+)R_\beta\begin{pmatrix}0&0\\0&M_{H^+}^2\end{pmatrix}R_\beta^{-1}\begin{pmatrix}\phi_1^+\\ \phi_2^+\end{pmatrix}+\frac{1}{2}(\xi_1,\xi_2)R_\beta\begin{pmatrix}0&0\\0&M_A^2\end{pmatrix}R_\beta^{-1}\begin{pmatrix}\xi_1\\ \xi_2\end{pmatrix}\\&+\frac{1}{2}(\eta_1,\eta_2)R_\beta\begin{pmatrix}M_{H_2^0}^2&0\\0&M_{H_1^0}^2\end{pmatrix}R_\beta^{-1}\begin{pmatrix}\eta_1\\ \eta_2\end{pmatrix},\end{aligned} \tag{B.7}$$

where the diagonalized matrix of neutral mass is $\mathrm{diag}(M_{H_2^0}^2,M_{H_1^0}^2)=R_\alpha\mathcal{M}^2R_\alpha^T$ with $(\mathcal{M}^2)_{ij}=\partial^2V/(\partial\eta_i\partial\eta_j)$. The mass eigenstates can then be expressed as follows:

$$\begin{pmatrix}G^+\\ H^+\end{pmatrix}=R_\beta^{-1}\begin{pmatrix}\phi_1^+\\ \phi_2^+\end{pmatrix},\quad \begin{pmatrix}G^0\\ A\end{pmatrix}=R_\beta^{-1}\begin{pmatrix}\xi_1\\ \xi_2\end{pmatrix},\quad \begin{pmatrix}H_2^0\\ H_1^0\end{pmatrix}=R_\alpha^{-1}R_\beta^{-1}\begin{pmatrix}\eta_1\\ \eta_2\end{pmatrix} \tag{B.8}$$

where

$$R_\beta=\begin{pmatrix}c_\beta&s_\beta\\ -s_\beta&c_\beta\end{pmatrix},\quad R_\alpha=\begin{pmatrix}c_\alpha&s_\alpha\\ -s_\alpha&c_\alpha\end{pmatrix}, \tag{B.9}$$

and with $-\pi/2\le\alpha\le\pi/2$. On this basis, G^+ and G^0 are massless Goldstone bosons which will become the longitudinal polarization of W^+ and Z^0 in the unitary gauge. The remaining terms $H^\pm$, A and $H_{1,2}^0$ are charged Higgs bosons, a CP-odd Higgs boson and CP-even Higgs bosons, respectively. Their masses are given by

$$M_{H^\pm}^2=\mu^2-\frac{v^2}{2}(\lambda_4+\lambda_5), \tag{B.10}$$

$$M_A^2=\mu^2-v^2\lambda_5, \tag{B.11}$$

$$M_{H_1^0}^2=s_\alpha^2\mathcal{M}_{11}^2-2s_\alpha c_\alpha\mathcal{M}_{12}^2+c_\alpha^2\mathcal{M}_{22}^2, \tag{B.12}$$

$$M_{H_2^0}^2=c_\alpha^2\mathcal{M}_{11}^2+2s_\alpha c_\alpha\mathcal{M}_{12}^2+s_\alpha^2\mathcal{M}_{22}^2. \tag{B.13}$$

Table B.1. All the couplings involving the decay processes $H \to \nu_l \bar{\nu}_l \gamma$.

Vertices	Couplings
$H_1^0 W_\mu^+ W_\nu^-$	$i\frac{2M_W^2}{v} s_{(\beta-\alpha)} g_{\mu\nu}$
$H_1^0(p) H^\pm(q) W_\mu^\mp$	$\mp i\frac{M_W}{v} c_{(\beta-\alpha)}\ (p-q)_\mu$
$H^+(p) H^-(q) A_\mu$	$i\frac{2M_W}{v} s_W\ (p-q)_\mu$
$H^+(p) H^-(q) Z_\mu$	$i\frac{M_Z}{v} c_{2W}\ (p-q)_\mu$
$H_1^0 H^+ H^-$	$\frac{i}{v}\Big[(2\mu^2 - 2M_{H^\pm} - M_{H_1^0}^2) s_{(\beta-\alpha)} + 2(\mu^2 - M_{H_1^0}^2)\cot 2\beta\ c_{(\beta-\alpha)}\Big]$

For the Higgs potential in Eq. (B.3) and the stationary conditions in Eq. (B.5), we have 7 parameters, which are

$$\left\{\lambda_{1,2,3,4,5}, t_\beta, m_{12}^2\right\}. \tag{B.14}$$

These parameters are equivalent to

$$\left\{M_{H^+}^2, M_A^2, M_{H_1^0}^2, M_{H_2^0}^2, \alpha, t_\beta, m_{12}^2\right\}. \tag{B.15}$$

These parameters will be used for phenomenological analysis. From the Higgs potential and kinematic term, we derive all the related couplings involving the decay processes $H \to \nu_l \bar{\nu}_l \gamma$ in this paper. Without loss of generality, we can consider the lightest Higgs boson H_1^0 as the SM like-Higgs boson. All the couplings are shown in Table B.1. For the Yukawa part, we refer the reader to Ref. [18] for more details. Depending on the types of THDMs, we then have the couplings of scalar fields and fermions. In this appendix, we mention the effective Lagrangian, which is the interactions of neutral Higgs (charged Higgs) with fermions. Taking τ-lepton and ν_τ as an example, we have the interaction terms

$$\mathcal{L}_{H_1^0 \tau\bar{\tau}} = \bar{\tau}\left(\lambda_\tau^L P_L + \lambda_\tau^R P_R\right)\tau H_1^0, \tag{B.16}$$

$$\mathcal{L}_{H^\pm \tau \nu_\tau} = \bar{\tau}\left(Y_\tau P_L + Y_{\nu_\tau} P_R\right)\nu_\tau H^+ + \bar{\nu_\tau}\left(Y_{\nu_\tau} P_L + Y_\tau P_R\right)\tau H^-. \tag{B.17}$$

It is noted that we are not going to present the explicit forms for the above couplings. They will be written explicitly in phenomenological analysis that will form our future works.

Appendix C. Feynman rules

In this appendix, Feynman rules for the decay channels $H \to \nu_l \bar{\nu}_l \gamma$ are presented for the most general extension of the SM, considering all possible contributions of additional heavy vector gauge bosons, fermions, and charged (and also neutral) scalar particles appearing in the loop diagrams. In this computation, V_i, V_j represents extra charged gauge bosons, V_k^0 is for neutral gauge bosons, $S_i, S_j (S_i^0)$ are charged (neutral) Higgs bosons and f_i,f_j are used for fermions. The propagators involving the decay processes in the unitary gauge are shown in Table C.1.

Table C.1. Feynman rules involving the decay in unitary gauge.

Particle types	Propagators
Fermions f	$i\frac{\not{k}+m_f}{k^2-m_f^2}$
Gauge boson V_i	$\frac{-i}{p^2-M_{V_i}^2}\left(g^{\mu\nu}-\frac{p^\mu p^\nu}{M_{V_i}^2}\right)$
Gauge boson V_k^0	$\frac{-i}{p^2-M_{V_k^0}^2+i\Gamma_{V_k^0}M_{V_k^0}}\left(g^{\mu\nu}-\frac{p^\mu p^\nu}{M_{V_k^0}^2}\right)$
Charged (neutral) scalar bosons $S_i(S_k^0)$	$\frac{i}{p^2-M_{S_i}^2(M_{S_k^0}^2)}$

In the most general extension of the SM, the full Lagrangian contains the following parts:

$$\mathcal{L}=\mathcal{L}_f+\mathcal{L}_G+\mathcal{L}_\Phi+\mathcal{L}_Y. \tag{C.1}$$

Where the fermion sector is given as

$$\mathcal{L}_f=\bar{\psi}_f i\not{D}\psi_f \tag{C.2}$$

with $D_\mu=\partial_\mu-igT^aV_\mu^a+\cdots$. In this formula, T^a is a generator of gauge symmetry. The gauge sector is expressed as

$$\mathcal{L}_G=-\frac{1}{4}\sum_a V_{\mu\nu}^a V^{a,\mu\nu}+\cdots, \tag{C.3}$$

where $V_{\mu\nu}^a=\partial_\mu V_\nu^a-\partial_\nu V_\mu^a+gf^{abc}V_\mu^bV_\mu^c$ with f^{abc} is the structure constant of the corresponding gauge group. The Higgs sector is described as follows:

$$\mathcal{L}_\Phi=\sum_\Phi Tr[\left(D_\mu\Phi\right)^\dagger\left(D^\mu\Phi\right)]-V(\Phi). \tag{C.4}$$

From the full Lagrangian, we then derive all the couplings. The structure of the couplings are explained by following.

- By expanding the fermion sector, we can derive the vertices of vector boson V with fermions. In detail, the interaction terms are parameterized as

$$\mathcal{L}_{Vff}=\sum_{f_i,f_j,V}\bar{f}_i\gamma^\mu(g_{Vff}^LP_L+g_{Vff}^RP_R)f_jV_\mu+\cdots. \tag{C.5}$$

- Trilinear gauge and quartic gauge couplings are extracted from the gauge sector:

$$\begin{aligned}\mathcal{L}_{VVV,VVVV}=&\sum_{V_k^0,V_i,V_j}g_{V_k^0V_iV_j}\Big[\partial_\mu V_{k,\nu}^0V_i^\mu V_j^\nu+V_{k,\nu}^0V_i^\mu\partial^\nu V_{j,\mu}+\cdots\Big]\\&+\sum_{V_k^0,V_l^0,V_i,V_j}g_{V_k^0V_l^0V_iV_j}\Big[V_{k,\mu}^0V_{l,\nu}^0V_i^\mu V_j^\nu+\cdots\Big]+\cdots.\end{aligned} \tag{C.6}$$

Table C.2. All couplings involving the decay processes in the unitary gauge.

Vertices	Couplings
$H \cdot \bar{f}_i \cdot f_j$	$-i\left(g^L_{Hf_if_j}P_L + g^R_{Hf_if_j}P_R\right)$
$A^\mu \cdot f_i \cdot \bar{f}_i$	$ieQ_f\gamma^\mu$
$V_k^{0\,\mu} \cdot f_i \cdot \bar{f}_j$	$i\gamma^\mu\left(g^L_{V_k^0 f_if_j}P_L + g^R_{V_k^0 f_if_j}P_R\right)$
$V_i^\mu \cdot \bar{l} \cdot \nu_l$	$i\gamma^\mu\left(g^L_{V_i l\nu_l}P_L + g^R_{V_i l\nu_l}P_R\right)$
$S_i \cdot \bar{l} \cdot \nu_l$	$ig^L_{S_i l\nu_l}P_L + ig^R_{S_i l\nu_l}P_R$
$S_i^* \cdot l \cdot \bar{\nu}_l$	$ig^R_{S_i l\nu_l}P_L + ig^L_{S_i l\nu_l}P_R$
$H \cdot V_i^\mu \cdot V_j^\nu$	$i\,g_{HV_iV_j}\,g^{\mu\nu}$
$H \cdot S_i \cdot S_j$	$-i\,g_{HS_iS_j}$
$H(p) \cdot V_i^\mu \cdot S_j(q)$	$i\,g_{HV_iS_j}\,(p-q)^\mu$
$A^\mu \cdot S_i^Q(p) \cdot S_i^{-Q}(q)$	$ieQ\,(p-q)^\mu$
$V_k^{0\,\mu} \cdot S_i(p) \cdot S_j(q)$	$i\,g_{V_k^0S_iS_j}\,(p-q)^\mu$
$V_k^{0\,\mu} \cdot V_i^\nu \cdot S_j$	$g_{V_k^0V_iS_j}\,g^{\mu\nu}$
$V_k^{0\,\mu}(p_1) \cdot V_i^\nu(p_2) \cdot V_j^\lambda(p_3)$	$-i\,g_{V_k^0V_iV_j}\,\Gamma^{\mu\nu\lambda}(p_1,p_2,p_3)$
$A^\mu(p_1) \cdot V_i^{Q\nu}(p_2) \cdot V_i^{-Q\lambda}(p_3)$	$-ieQ\,\Gamma^{\mu\nu\lambda}(p_1,p_2,p_3)$
$V_k^{0\,\mu} \cdot A^\nu \cdot V_i^\alpha \cdot V_j^\beta$	$-i\,g_{V_k^0AV_iV_j}\,S^{\mu\nu,\alpha\beta}$

- We can derive the couplings of the scalar S to fermions from the Yukawa part $\mathcal{L}_Y$. The interaction term is presented as follows:

$$\mathcal{L}_{Sf_if_j} = \sum_{f_i,f_j,S} \bar{f}_i(g^L_{Sff}P_L + g^R_{Sff}P_R)f_jS + \cdots . \tag{C.7}$$

- From the kinematic term of the Higgs sector, one can derive the coupling of the scalar S to the vector boson V. In detail, we have the interaction terms

$$\begin{aligned}\mathcal{L}_{SVV,SSV,SSVV} = &\sum_{S,V_i,V_j} g_{SV_iV_j}SV_i^\mu V_{j,\mu} + \sum_{S_i,S_j,V} g_{S_iS_jV}[(\partial_\mu S_i)S_j - (\partial_\mu S_j)S_i]V^\mu \\ &+ \sum_{S_i,S_j,V_k,V_l} g_{S_iS_jV_kV_l}S_iS_jV_k^\mu V_{l,\mu} + \cdots\end{aligned} \tag{C.8}$$

- Finally, the trilinear scalar and quartic scalar interactions are from the Higgs potential $V(\Phi)$:

$$\mathcal{L}_{SSS,SSSS} = \sum_{S_i,S_j,S_k} g_{S_iS_jS_k} S_iS_jS_k + \sum_{S_i,S_j,S_k,S_l} g_{S_iS_jS_k,S_l} S_iS_jS_kS_l + \cdots \tag{C.9}$$

All the related couplings involving the decay channels are parameterized in general forms which are presented in Table C.2 (also see Appendix B for a typical example). We use $P_{L/R} = (1 \mp \gamma_5)/2$, $\Gamma^{\mu\nu\lambda}(p_1,p_2,p_3) = g^{\mu\nu}(p_1 - p_2)^\lambda + g^{\lambda\nu}(p_2 - p_3)^\mu + g^{\mu\lambda}(p_3 - p_1)^\nu$ and $S^{\mu\nu,\alpha\beta} = 2g^{\mu\nu}g^{\alpha\beta} - g^{\mu\alpha}g^{\nu\beta} - g^{\mu\beta}g^{\nu\alpha}$, and Q denotes the electric charge of the gauge bosons V_i^Q and charged Higgs bosons S^Q.

References

[1] A. Liss and J. Nielsen [ATLAS Collaboration], arXiv:1307.7292 [hep-ex] [Search INSPIRE].
[2] CMS Collaboration, arXiv:1307.7135 [hep-ex] [Search INSPIRE].
[3] H. Baer et al., arXiv:1306.6352 [hep-ph] [Search INSPIRE].
[4] A. M. Sirunyan et al. [CMS Collaboration], Phys. Lett. B **793**, 520 (2019).
[5] M. Aaboud et al. [ATLAS Collaboration], Phys. Rev. Lett. **122**, 231801 (2019).
[6] M. Aaboud et al. [ATLAS Collaboration], Phys. Lett. B **793**, 499 (2019).
[7] V. S. Ngairangbam, A. Bhardwaj, P. Konar, and A. K. Nayak, Eur. Phys. J. C **80**, 1055 (2020).
[8] G. Aad et al. [ATLAS Collaboration], Eur. Phys. J. C **72**, 1844 (2012).
[9] G. Bélanger, B. Dumont, U. Ellwanger, J. F. Gunion, and S. Kraml, Phys. Lett. B **723**, 340 (2013).
[10] M. Heikinheimo, K. Tuominen, and J. Virkajärvi, J. High Energy Phys. **1207**, 117 (2012).
[11] A. M. Sirunyan et al. [CMS Collaboration], J. High Energy Phys. **1910**, 139 (2019).
[12] A. M. Sirunyan et al. [CMS Collaboration], J. High Energy Phys. **2103**, 011 (2021).
[13] Y. Sun and D.-N. Gao, Phys. Rev. D **89**, 017301 (2014).
[14] J. F. Kamenik and C. Smith, Phys. Rev. D **85**, 093017 (2012).
[15] H. Davoudiasl, H.-S. Lee, I. Lewis, and W. J. Marciano, Phys. Rev. D **88**, 015022 (2013).
[16] D. Curtin, et al. Phys. Rev. D **90**, 075004 (2014).
[17] C. Petersson, A. Romagnoni, and R. Torre, J. High Energy Phys. **1210**, 016 (2012).
[18] G. C. Branco, P. M. Ferreira, L. Lavoura, M. N. Rebelo, M. Sher, and J. P. Silva, Phys. Rept. **516**, 1 (2012).
[19] J. C. Pati and A. Salam, Phys. Rev. D **10**, 275 (1974); **11**, 703 (1975) [erratum].
[20] R. N. Mohapatra and J. C. Pati, Phys. Rev. D **11**, 2558 (1975).
[21] G. Senjanovic and R. N. Mohapatra, Phys. Rev. D **12**, 1502 (1975).
[22] M. Singer, J. W. F. Valle, and J. Schechter, Phys. Rev. D **22**, 738 (1980).
[23] J. W. F. Valle and M. Singer, Phys. Rev. D **28**, 540 (1983).
[24] F. Pisano and V. Pleitez, Phys. Rev. D **46**, 410 (1992).
[25] P. H. Frampton, Phys. Rev. Lett. **69**, 2889 (1992).
[26] R. A. Diaz, R. Martinez, and F. Ochoa, Phys. Rev. D **72**, 035018 (2005).
[27] R. M. Fonseca and M. Hirsch, J. High Energy Phys. **1608**, 003 (2016).
[28] R. Foot, H. N. Long, and T. A. Tran, Phys. Rev. D **50**, R34(R) (1994).
[29] L. A. Sánchez, F. A. Pérez, and W. A. Ponce, Eur. Phys. J. C **35**, 259 (2004) [arXiv:hep-ph/0404005] [Search INSPIRE].
[30] W. A. Ponce and L. A. Sánchez, Mod. Phys. Lett. A **22**, 435 (2007) [arXiv:hep-ph/0607175] [Search INSPIRE].
[31] Riazuddin and Fayyazuddin, Eur. Phys. J. C **56**, 389 (2008) [arXiv:0803.4267 [hep-ph]] [Search INSPIRE].
[32] A. Jaramillo and L. A. Sánchez, Phys. Rev. D **84**, 115001 (2011) [arXiv:1110.3363 [hep-ph]] [Search INSPIRE].
[33] H. N. Long, L. T. Hue, and D. V. Loi, Phys. Rev. D **94**, 015007 (2016) [arXiv:1605.07835 [hep-ph]] [Search INSPIRE].
[34] A. Denner and S. Dittmaier, Nucl. Phys. B **734**, 62 (2006).
[35] T. Hahn and M. Pérez-Victoria, Comput. Phys. Commun. **118**, 153 (1999).
[36] A. Kachanovich, U. Nierste, and I. Nišandžić, Phys. Rev. D **101**, 073003 (2020).
[37] H. H. Patel, Comput. Phys. Commun. **197**, 276 (2015).